Theory of the band-gap anomaly in ABC_2 chalcopyrite semiconductors

J. E. Jaffe and Alex Zunger

Solar Energy Research Institute, Golden, Colorado 80401

(Received 12 September 1983)

Using self-consistent band-structure methods, we analyze the remarkable anomalies ($>50\%$) in the energy-band gaps of the ternary IB-IIIA-VIA_2 chalcopyrite semiconductors (e.g., CuGaS$_2$) relative to their binary zinc-blende analogs IIB-VIA (e.g., ZnS), in terms of a chemical factor ΔE_g^{chem} and a structural factor ΔE_g^S. We show that ΔE_g^{chem} is controlled by a p-d hybridization effect ΔE_g^d and by a cation electronegativity effect ΔE_g^{CE}, whereas the structural contribution to the anomaly is controlled by the existence of bond alternation ($R_{AC} \neq R_{BC}$) in the ternary system, manifested by nonideal anion displacements $u - \frac{1}{4} \neq 0$. All contributions are calculated self-consistently from band-structure theory, and are in good agreement with experiment. We further show how the nonideal anion displacement and the cubic lattice constants of all ternary chalcopyrites can be obtained from elemental coordinates (atomic radii) without using ternary-compound experimental data. This establishes a relationship between the electronic anomalies and the atomic sizes in these systems.

I. INTRODUCTION

The ternary ABC_2 chalcopyrites (A =Cu and Ag, B=Al, Ga, and In, and C=S, Se, and Te) form a large group of semiconducting materials with diverse optical, electrical, and structural properties.[1-8] One of them—CuInSe$_2$—has recently emerged as a very promising material for photovoltaic solar-energy applications,[9-11] due partly to the fact that it is probably the strongest absorbing semiconductor under sunlight[12-14] (cf., Fig. 1). One can define a binary analog to each ternary compound by taking the cation that is situated in the Periodic Table between the A and B atoms (e.g., ZnS is the binary analog of CuGaS$_2$, or Zn$_{0.5}$Cd$_{0.5}$S is the binary analog of CuInS$_2$). Despite the overall structural similarity between the ternary I-III-VI$_2$ compounds and their II-VI binary analogs, the band gaps of the former compounds are substantially smaller than those of the latter. This can be seen in Table I,[8,15-25] which depicts the band-gap anomaly ΔE_g, defined as the difference between the binary gap $E_g^{(2)}$ and the ternary gap $\Delta E_g^{(3)}$. In fact, it is this strong red shift of the ternary band gap that makes some of the ABC_2 compounds such strong absorbers of sunlight (Fig. 1).

In addition to this electronic anomaly, ternary chalcopyrites have also some interesting structural anomalies[24,26] relative to their binary analogs (see Fig. 2 for comparison of the crystal structures). First, rather than have a single cation, the ternary chalcopyrites have two cations; starting from the A atom and translating in the vertical direction in Fig. 2 through intervals of $c/2$ we find the sequence $ABAB \cdots$, whereas translating horizontally with an interval of a, we find the sequence $AAA \cdots$. Second, these crystals often show a tetragonal distortion where the ratio between the lattice parameters $\eta \equiv c/2a$ (tetragonal deformation) differ from 1 by as much as 12%. Third, the anions are displaced from their zinc-blende sites. This reflects the fact that in binary AC

zinc-blende compounds each cation A has four anions C as nearest neighbors (and vice versa), whereas in a ternary chalcopyrite ABC_2 each cation A and B has four anions C as nearest neighbors, and each anion has two A and two B cations as nearest neighbors. As a result, the anion C usually adopts an equilibrium position closer to one pair of cations than to the other, that is, unequal bond lengths $R_{AC} \neq R_{BC}$ (bond alternation). The nearest-neighbor anion-cation bond lengths are given by

$$R_{AC} = [u^2 + (1+\eta^2)/16]^{1/2}a$$

and   (1)

$$R_{BC} = [(u-\tfrac{1}{2})^2 + (1+\eta^2)/16]^{1/2}a .$$

Hence, the anion displacement $u - \frac{1}{4} = (R_{AC}^2 - R_{BC}^2)/a^2$ measures the extent of bond alternation in the system. Table II (Refs. 27–48) gives a compilation of the experimental data for a, η, and u of ternary ABC_2 semiconductors. The structural anomalies $\eta - 1$ and $u - \frac{1}{4}$ relative to the zinc-blende structure ($\eta = 1$ and $u = \frac{1}{4}$) are seen to be significant. Note that the anion position parameter u is often called x of x_f in the literature, and one also encounters notations such as $\sigma = 4u - 1$ and $\epsilon = 2(1-\eta)$.

We have recently completed a detailed series of self-consistent band-structure calculations for the six Cu chalcopyrites[26] (A=Cu, B=Al, Ga, and In, and C=S and Se) in their equilibrium crystal structure, in which we have studied the trends in the one-electron energies and chemical bonding along this series. In the present study, we focus on the relationships between the band-gap anomaly (Table I) and the structural anomalies relative to binary compounds (Table II). While on the simplest phenomenological level one could dispose of the issue by taking the viewpoint that both the band-gap and the structural anomalies in the ternary compounds relative to their binary analogs ultimately arise from the differences between the A and B atoms and the zinc-blende cation, our
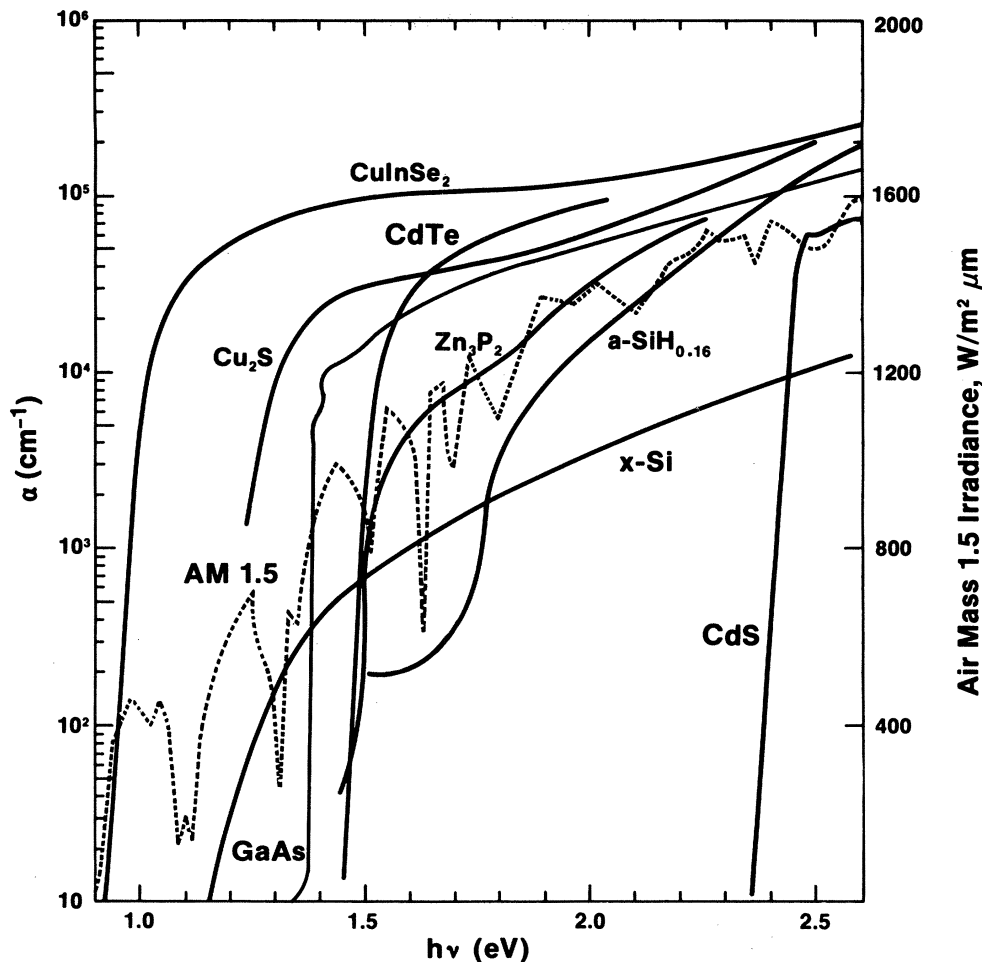
FIG. 1. Absorption spectrum (Ref. 12) of $CuInSe_2$ compared with that of other photovoltaic semiconductors (Ref. 13). For comparison, we give also the air mass (AM) 1.5 solar-emission spectrum (Ref. 14). a-$SiH_{0.16}$ is amorphous hydrogenated Si and x-Si is crystalline Si.

aim here will be to analyze this statement in terms of well-defined chemical constructs (hybridization, electronegativities, and bond-length mismatch) with the hope that such an analysis would also provide predictive insights for controlling the material properties of such compounds. We will use $CuInSe_2$ as our prototype system. In Sec. II we will briefly describe the theoretical tools used to compute self-consistently the electronic band structure of these materials. We will discuss the general features of the electronic bands, charge densities, and bonding for the equilibrium crystal structure used later in our discussion of structurally and chemically driven electronic anomalies. We will show that the band-gap anomaly can be analyzed in terms of (i) a p-d hybridization effect (Sec. III), (ii) a cation-electronegativity effect (Sec. IV), and (iii) a structural effect (Sec. V). In Sec. VI we will discuss these three effects and their additivity. Having established that the anion displacements control the structural part of the band-gap anomaly, in Sec. VII we will analyze the elemental factors (size mismatch between atomic radii) that control the anion displacements. This will establish a relation between the (semiclassical) structural coordinates (atomic radii) and the structurally driven electronic anomaly. In Sec. VIII we provide predictions of structural parameters

and band gaps for ternary chalcopyrites that have not yet been observed, while Sec. IX constitutes a summary.
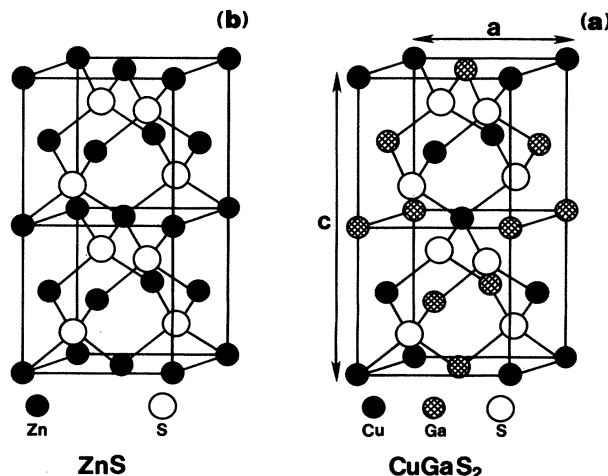
FIG. 2. Crystal structure of (a) chalcopyrite and (b) zinc-blende lattices.

TABLE I. Band gaps of ternary semiconductors $E_g^{(3)}$ and the difference $\Delta E_g \equiv E_g^{(2)} - E_g^{(3)}$ (band-gap anomaly) with respect to the binary analogs. $E_g^{(3)}$ values are compiled from Refs. 8 and 15–22, and correspond to room temperature, except as noted. The binary band gaps $E_g^{(2)}$ are from Ref. 23 taken at the corresponding temperatures. Uncertain values are denoted by an asterisk.

Ternary	Ternary band gap $E_g^{(3)}$ (eV)	Binary analog	Band-gap anomaly ΔE_g (eV)
CuAlS₂	3.49[a]	Mg₀.₅Zn₀.₅S	2.41
CuGaS₂	2.43[b]	ZnS	1.37
CuInS₂	1.53[b]	Zn₀.₅Cd₀.₅S	1.64
CuAlSe₂	2.67[c]	Mg₀.₅Zn₀.₅Se	1.47
CuGaSe₂	1.68[a]	ZnSe	1.00
CuInSe₂	1.04[d]	Zn₀.₅Cd₀.₅Se	1.29
CuAlTe₂	2.06[e]	Mg₀.₅Zn₀.₅Te	1.44
CuGaTe₂	1.23[f]	ZnTe	1.06
CuInTe₂	0.96[g]–1.06[h]	Zn₀.₅Cd₀.₅Te	0.98–0.88
AgAlS₂	3.13[e]		
AgGaS₂	2.51[e]–2.73[i]	Zn₀.₅Cd₀.₅S	0.62–0.44
AgInS₂	1.87[j]	CdS	0.66
AgAlSe₂	2.55[e]		
AgGaSe₂	1.83[i]	Zn₀.₅Cd₀.₅Se	0.50
AgInSe₂	1.24[d]	CdSe	0.61
AgAlTe₂	2.27[k*]		
AgGaTe₂	1.1[g]–1.326[k*]	Zn₀.₅Cd₀.₅Te	0.84–0.62
AgInTe₂	0.96[g]–1.04[k*]	CdTe	0.62–0.54

[a]Reference 15; single crystal.
[b]Reference 16; single crystal.
[c]Reference 17; single crystal.
[d]Reference 18; 77 K, single crystal.
[d]Reference 19; single crystal.
[e]Reference 19; single crystal.
[f]Reference 20; thin-film sample.
[g]Reference 8, p. 336; temperature and sample type not given.
[h]Reference 21; single crystal.
[i]Reference 22; single crystal.
[j]Reference 3, p. 118; single crystal.
[k]Reference 7, p. 165; 77 K, sample type not given.

II. CALCULATING THE BAND STRUCTURE

A. Computational strategy

We calculate the electronic structure of ternary chalcopyrites in the local-density approach using the potential-variational-mixed-basis (PVMB) method described before.[26,49] In this approach, the effective one-body Kohn-Sham (KS) potential is given as

$$V_{KS}[\rho(\vec{r})] = V_{ext}(\vec{r}) + \int d\vec{r}\, \frac{\rho(\vec{r}')}{|\vec{r} - \vec{r}'|} + \frac{\delta E_{xc}[\rho(\vec{r})]}{\delta \rho(\vec{r})}$$

$$= V_{ext}(\vec{r}) + V_{Coul}[\rho(\vec{r})] + V_{xc}[\rho(\vec{r})], \quad (2)$$

where $V_{ext}(\vec{r})$ is the external potential (interpreted in our all-electron approach as the electron-nuclear potential), $\rho(\vec{r})$ is the ground-state charge density, V_{Coul} is the interelectronic Coulomb repulsion, and V_{xc} is the exchange-correlation potential for which we have used both Ceperley's form,[50,51] as given by Perdew and Zunger,[52] and the Slater form, but with an exchange coefficient of $\alpha = 1.1$ (see below). The main characteristics of the nonrelativistic PVMB method are as follows. (1) The single-particle wave functions $\psi_j(\vec{r})$ are generated through the potential gradient approach in which the conventional wave-function gradient variational principle $\partial E/\partial \psi = 0$ is replaced by the equivalent (but computationally more tractable) condition $\partial E/\partial \mu_i = 0$, where E is the total energy and the μ are variational parameters of the generating potential[49] $U(\{\mu\}; \vec{r})$. (2) The wave functions are expanded in a mixed-basis set consisting of coordinate-space compressed atom orbitals and plane waves. (3) No shape approximations (muffin tin or other) are applied to the potential; the Hamiltonian matrix is generated from the potential in Eq. (2) and the prescribed basis set, essentially with no approximations except for convergence criteria which are monitored to achieve a prescribed tolerance of precision. (4) The residual minimization direct inversion in the iterative subspace (RM DIIS) method[53] is used for diagonalizing the Hamiltonian matrix; this method is far more efficient than the conventional Hausholder-Choleski approach, provides arbitrarily precise eigensolutions, and permits efficient handling of large matrices (about 800×800 in our case) without requiring their storage. (5) The charge density is computed by sampling the wave functions at special points in the irreducible Brillouin zone (in the present study, a single $\vec{k}$ point). (6) Accelerated self-consistency is obtained by using the Newton-Raphson Jacobian update method[49] to a tolerance of 1–3 mRy. Convergence studies with respect to all internal computational parameters were carried out;[26,49] we select convergence tolerances that produce a precision of ~0.15 eV in the band energies in a region of ±10 eV around the Fermi energy E_F.

B. Band structure

Figure 3 displays the band structure of CuInSe₂ as calculated with (a) Ceperley's correlation and (b) the Slater exchange. Figure 4 depicts the density of states produced by both approaches. Whereas Ceperley's correlation produces a one-electron spectrum that correlates well[26] with the photoemission data, it fails to reproduce the observed band gap[54] [~1 eV(Ref. 18)]. The chemical trends in the electronic charge densities of six CuBC_2 chalcopyrites (B=Al, Ga, and In, and C=S and Se) using Ceperley's correlation have been discussed previously.[26] Since, however, in the present study, we are interested in studying the *changes* in the electronic band gaps induced by structural variations, the misrepresentation of the band gap by Ceperley's correlation constitutes a serious handicap. We seek, therefore, a simple empirical adjustment that will correct the band gaps of those chalcopyrites while approximately preserving the derivatives $\partial \Delta \epsilon / \partial \lambda$ of the one-electron energy gaps $\Delta \epsilon$ with structural parameters λ

TABLE II. Compilation of the experimental structural parameters a and c (lattice constants, measured in Å), u (anion displacement), and $2\eta \equiv c/a$ (tetragonal deformation) for the ternary ABC_2 system. The numbers in parentheses are uncertainties in the last digits. All values are taken at or near room temperature. The spread in values is often due to slight nonstoichiometry. Values of c/a are quoted directly from the experimental work even if they are slightly inconsistent with the values of c and a given in the same work. The calculated values u_{calc} are from the "CTB plus $\eta = \eta_{tet}$ rule," using Pauling radii, and are described in Sec. VII A. In most cases, only those references are included that contain a measured value for u; the values of u given in Ref. 27 appear doubtful since they agree poorly with other measurements as well as with theory.

Compound	a (Å)	c (Å)	c/a	u	Ref.	u_{calc}
		I-III-VI$_2$ Chalcopyrites				
CuAlS$_2$	5.31(2)	10.42	1.961	0.27	27	
	5.334(1)	10.444(2)	1.958	0.275(2)	28	0.264
	5.3336(5)	10.444(2)	1.958	0.268(4)	29	
CuAlSe$_2$	5.606	10.90	1.945	0.26	27	
	5.602(2)	10.944(5)	1.954	0.269(5)	28	0.264
CuAlTe$_2$	5.964	11.78	1.975	0.25	27	0.263
CuGaS$_2$	5.349	10.47	1.958	0.25	27	
	5.356(1)	10.435(5)	1.948	0.275(5)	28	
	5.347 41(7)	10.474 29(6)	1.958 76	0.2539(4)	30	0.264
	5.351(1)	10.480(5)	1.9586	0.272(5)	31	
CuGaSe$_2$	5.607	10.99	1.960	0.25	27	
	5.614(1)	11.03(1)	1.965	0.250(1)	28	0.264
	5.5963(1)	11.00 36(2)	1.96623	0.2431(2)	32	
CuGaTe$_2$	5.994	11.91	1.987	0.25	27	0.263
CuInS$_2$	5.517	11.06	2.005	0.20	27	
	5.523(4)	11.12(2)	2.013	0.214(7)	28	0.236
	5.522 79(7)	11.132 95(22)	2.015 82	0.2295(4)	30	
CuInSe$_2$	5.773	11.55	2.001	0.22	27	
	5.784(1)	11.616(5)	2.008	0.224(3)	28	0.237
	5.782	11.620	2.009 69	0.235(5)	33	
CuInTe$_2$	6.167	12.34	2.000	0.225	27	0.237
CuTlS$_2$	5.580	11.17	2.001	0.19	27	0.231
CuTlSe$_2$	5.832	11.63	1.995	0.23	27	0.232
AgAlS$_2$	5.695	10.26	1.802	0.30	27	
	5.720(1)	10.135(10)	1.772	0.290(3)	28	0.288
AgAlSe$_2$	5.956	10.75	1.805	0.27	27	
	5.986(1)	10.70(1)	1.793		28	0.287
AgAlTe$_2$	6.296	11.83	1.878	0.26	27	0.285
AgGaS$_2$	5.743	10.26	1.786	0.28	27	
	5.754(2)	10.295(6)	1.789	0.304(6)	28	0.288
	5.757 22(3)	10.3036(2)	1.789 68	0.2908(4)	34	
AgGaSe$_2$	5.973	10.88	1.823	0.27	27	
	5.985(2)	10.73(1)	1.793	0.276(3)	28	0.287
AgGaTe$_2$	6.283	11.94	1.897	0.26	27	0.285
AgInS$_2$	5.816	11.17	1.920	0.25	27	
	5.872(1)	11.214(3)	1.910	0.250(1)	28	0.262

TABLE II. (*Continued.*)

Compound	a (Å)	c (Å)	I-III-VI$_2$ Chalcopyrites c/a	u	Ref.	u_{calc}
AgInSe$_2$	6.090	11.67	1.916	0.25	27	
	6.109(1)	11.717(5)	1.919	0.250(1)	28	0.261
	6.1038(15)	11.7118(47)	1.918 77	0.258 45(16)	35	
AgInTe$_2$	6.406	12.56	1.962	0.25	27	0.2608
		Transition-metal-containing chalcopyrites				
CuFeS$_2$	5.25	10.32	1.91	0.27	8	0.269
	5.2988	10.434	1.969		36	
AgFeS$_2$	5.67	10.32	1.82		8	0.293
		II-IV-V$_2$ Pnictides				
ZnSiP$_2$	5.399(1)	10.435(2)	1.932 77	0.2691(4)	37	0.272
	5.399	10.436	1.933	0.271	38	
ZnSiAs$_2$	5.60(1)	10.88(1)	1.94	0.265 75(12)	39	0.271
	5.611	10.885	1.940	0.269	38	
ZnGeP$_2$	5.465	10.700	1.958	0.267	38	
	5.46(1)	10.71(1)	1.96	0.258 16(44)	39	0.264
	5.466	10.722	1.961	0.264	8	
	5.46(1)	10.758	1.97(1)		47	
ZnGeAs$_2$	5.672	11.153	1.967(2)	0.264	8	0.264
	5.672	11.151	1.966	0.250	38	
ZnSnP$_2$	5.651	11.302	2.00	0.239	40	0.236
ZnSnAs$_2$	5.851	11.702	2.00	0.231	38	
	5.851(1)	11.702	2.00	0.23[a]	41	0.236
	5.852(1)	11.705(1)	2.00	0.239	42	
ZnSnSb$_2$	6.275	12.550	2.00	0.228	43	0.237
	≤6.273	12.546	2.00	≤0.228	38	
CdSiP$_2$	5.680(1)	10.431(3)	1.836 44	0.2967(2)	44	0.296
	5.678	10.430	1.837	0.302	38	
CdSiAs$_2$	5.885	10.881	1.849	0.298	45,38	0.294
CdGeP$_2$	5.740	10.775	1.8772	0.283	46,38	0.288
CdGeAs$_2$	5.9432(1)	11.2163(3)	1.887 25	0.2785(2)	32	
	5.942(2)	11.2244	1.889(2)	0.285(5)	36	0.287
	5.945	11.212	1.886	10.280	48,38	
CdSnP$_2$	5.901	11.513	1.951	0.265	38	0.262
CdSnAs$_2$	6.093	11.936	1.96	0.261	8	0.261
	6.094	11.920	1.956	0.262	38	
MgSiP$_2$	5.718	10.115	1.769	0.292	38	0.284

[a]Our extrapolation from the author's x-ray data.

(anion displacements, tetragonal distortions, etc.), as obtained with the Ceperley correlation. We find empirically that scaling the exchange potential (with an exchange coefficient $\alpha = \frac{2}{3}$) by 1.65 (i.e., an exchange coefficient of $\alpha = 1.1$) satisfies these conditions to within a good approximation: This single adjustable parameter produces band gaps of all six chalcopyrites within ~ 0.2 eV of experiment [e.g., for CuInSe$_2$ the calculated gap is 0.985 eV, compared with the observed value of 0.98—1.04 eV (Refs. 12 and 18)], while the structural derivatives are within
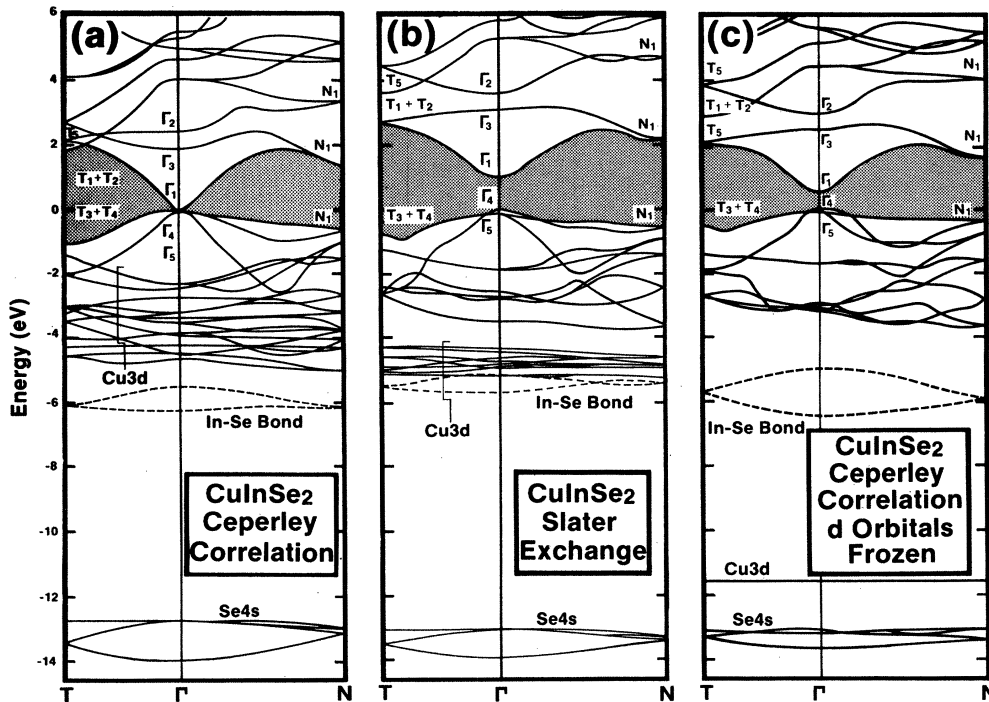
FIG. 3. Self-consistent band structure of $CuInSe_2$ calculated at the observed crystal structure $a = 10.9303$ a.u., and $u = 0.224$ and $\eta = 1.004$, using (a) the Ceperley correlation (Refs. 51 and 52), (b) Slater-type exchange with $\alpha = 1.1$, and (c) Ceperley's correlation but freezing the Cu d orbitals. The shaded areas denote the principal band gap.

10—15% of those obtained with Ceperley's correlation. While the need for such an empirical adjustment reflects the inability of the state of the art first-principles local-density calculations to *predict* electronic excitation energies in complex condensed systems with sufficient accuracy,[52,54] we believe that the choice of an adjustment that preserves the derivatives of the energies is adequate for the limited purpose of studying structurally induced changes in the electronic properties.

C. Electronic structure of the undeformed crystal

Here we describe the band structure and the electronic charge distribution in $CuInSe_2$ as obtained in the scaled-exchange calculation at the observed crystal structure (the results for the Ceperley exchange-correlation were described before[26,49]). The electronic band structure shows a few major subbands below E_F. First, in the region of 0 to -4 eV below the valence-band maximum (VBM), the upper valence band consists of Se p and Cu d states. Figure 5(a) depicts the electronic charge density in this subband, where the contours around the Cu—Se contact are shaded to highlight the formation of the bonding Cu d—Se p contact and the nonbonding character of the In—Se contact. Second, in the energy region $E_{VBM} - 4.3$ to $E_{VBM} - 5.4$ eV, we find the In—Se band (dashed lines in Fig. 3) and the densely spaced Cu $3d$ bands. The charge

density of these subbands [Fig. 5(b)] shows the formation of a weak In—Se bond (where a partially covalent bond charge is formed at the In—Se contact, but is ionically polarized towards the Se site) and a nearly spherical (i.e., closed-shell) charge on the Cu site. These subbands show up as a distinct peak in the density of states near $E_{VBM} - 4.5$ eV [Fig. 4(b)]. Third, in the region between $E_{VBM} - 13$ to $E_{VBM} - 14$ eV, we find the Se $4s$ subband showing up as a sharp peak in the density of states (Fig. 4), and having an extended s-like charge distribution around the Se site [Fig. 5(c)].

The total ground-state charge density in $CuInSe_2$ is shown in Fig. 6, both as a contour plot [Fig. 6(a)] and as line plots along the Cu—Se [Fig. 6(b)] and In—Se bonds [Fig. 6(c)]. Our model describes the bonding in the system as mixed ionic and covalent where the In site is isolated from its nearest-neighbor Se sites by nodes, whereas the charge on the Cu atom merges continuously into that of the nearest-neighbor Se sites forming a partially covalent bond charge closing around both atoms.

III. EFFECTS OF d BONDING ON THE BAND GAP

Shay and Kasper[55] have pointed out that the anomalous reduction in the band gaps of ternary chalcopyrites relative to their binary analogs is correlated with the existence of d bonding in the former compounds. They found that the band-gap anomaly ΔE_g correlates nearly linearly with the percentage of d character α_d deduced by comparing
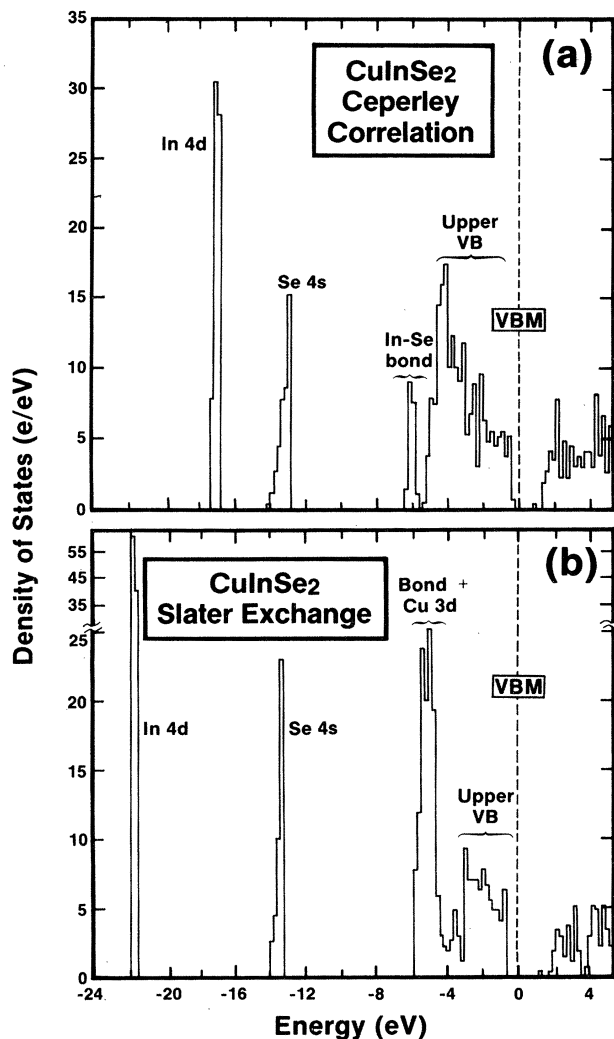
FIG. 4. Density of states of $CuInSe_2$ calculated with (a) Ceperley's correlation and (b) Slater-type exchange with $\alpha = 1.1$. The latter exchange parameter was chosen to fit the optical gap to experiment.

the spin-orbit splitting of the ternary and binary compounds, i.e., $\Delta E_g = a\alpha_d$ with $a \simeq 3.125$ eV. They have suggested that $CuAlS_2$, $CuGaS_2$, $CuGaSe_2$, and $CuInSe_2$ have a nearly constant percentage of d character ($\alpha_d = 35\%$, 35%, 36%, and 34%, respectively), whereas $CuInS_2$, with a large band-gap anomaly of 1.6 eV, has the largest percentage of d character (45%) in this group. Their analysis appears, however, to be incomplete in three respects. First, $CuAlS_2$ (not shown in their correlation[55]) has even a larger band-gap anomaly (~ 2.4 eV) than $CuInS_2$, leading, by the Shay-Kasper correlation, to 77% d character, far larger than the value of 35% determined by them from the spin-orbit splitting. Second, the deduction of the percentage of d character from the differences in spin-orbit splittings of binary and ternary compounds is at best ambiguous due to the substantial differences in bond angles around the anion (determining the proportions of hybridization) between the two. Third, the interpretation of trends in ΔE_g in different chalcopyrites as arising *solely* from a chemical factor (d mixing) overlooks
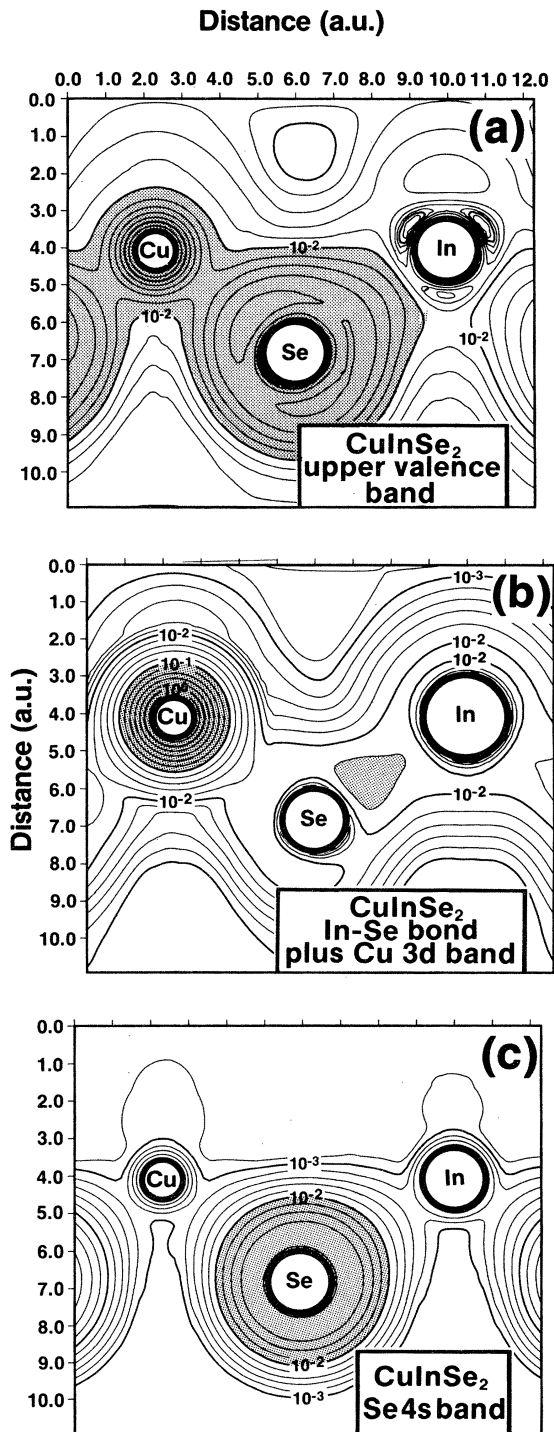
FIG. 5. Charge densities, in units of $e/\text{a.u.}^3$, of the three major valence subbands of $CuInSe_2$, calculated with Slater-type exchange. The contours are logarithmically spaced; the areas inside the solid circles denote atomic cores where the rapidly varying charge density has been omitted, for clarity. (a) The upper valence band. The 10^{-2} $e/\text{a.u.}^3$ contours around the Cu—Se bond are shaded to highlight the partially covalent bond. (b) The In—Se and Cu d subbands. The shading highlights the formation of a bond charge on the In—Se contact (ionically polarized towards the anion) and the nearly spherical Cu closed-shell charge. (c) The Se s subband. The 10^{-2} $e/\text{a.u.}^3$ contours around Se are shaded to highlight the extended Se s charge.
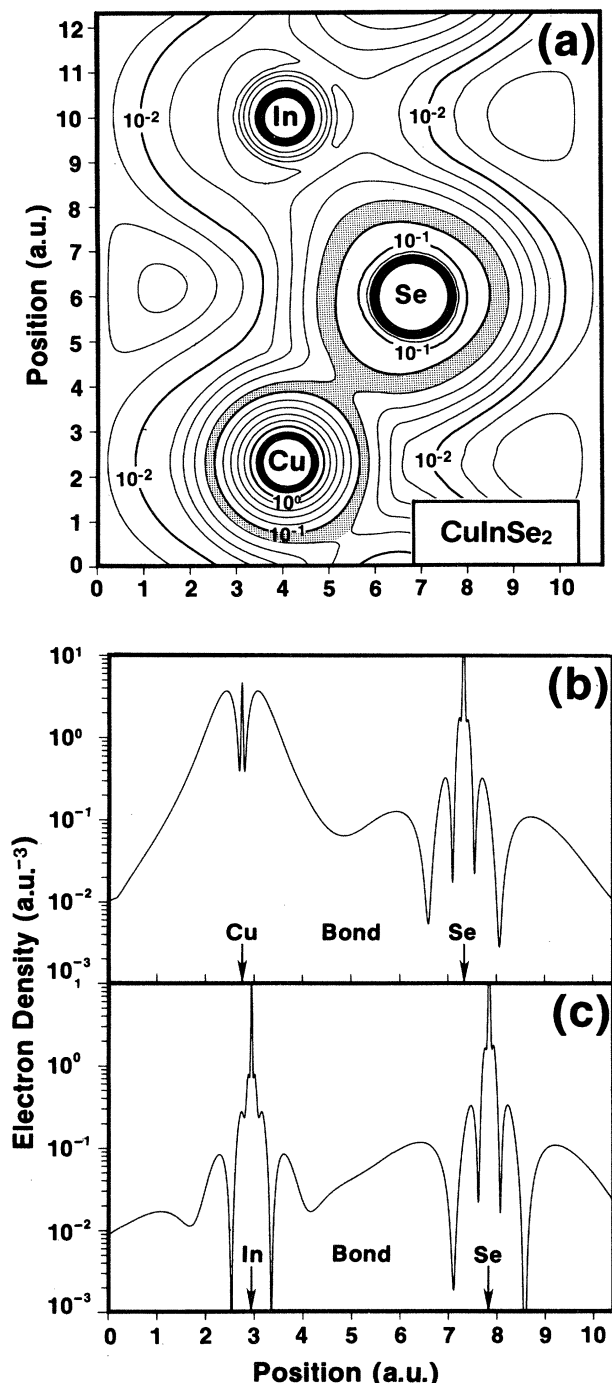
FIG. 6. Total valence charge density of $CuInSe_2$ calculated with Slater-type exchange. (a) Logarithmically spaced contour plot with shading highlighting the formation of a covalent lobe around the Cu-Se contact. (b) and (c) display line plots along the Cu—Se and In—Se bonds, respectively.

the significance of the structural factor (substantial differences in anion displacements) which partially control p-d hybridization, and hence α_d.

A quantum-mechanical description of the electronic structure of a solid in terms of atomic orbitals permits one to assess unambiguously the influence of a given atomic subshell on the global electronic structure of the compound. We have performed a self-consistent PVMB cal-
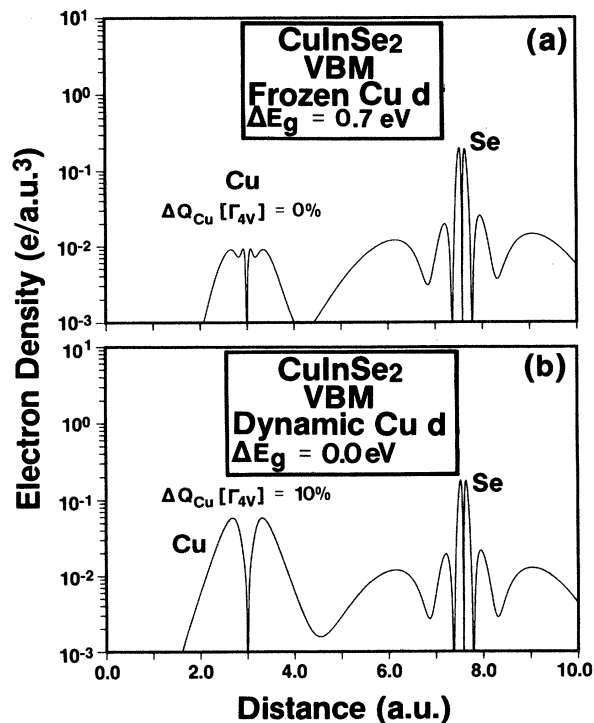
FIG. 7. Effect of freezing the Cu d orbitals on the charge density of $CuInSe_2$ at the VBM. (a) Frozen d orbitals, and (b) dynamic d orbitals. ΔE_g denotes the change in the direct band gap due to d-orbital effects and $\Delta Q_{Cu}[\Gamma_{4v}]$ denotes the change in the percentage of Cu d character at the VBM upon unfreezing the d orbitals. Note that freezing the d orbitals reduces the bond charge along the Cu—Se contact, diminishes the Cu d character, and opens up the band gap by 0.7 eV.

culation of the band structure of $CuInSe_2$ in its observed crystal structure where the atomic Cu $3d$ orbitals are frozen, i.e., all other electrons move in an external potential $V_{ext}(\vec{r})$ [Eq. (2)] which contains, this time, the field of the (compressed[48]) Cu $3d$ states. Figure 3(c) depicts the band structure of $CuInSe_2$ with frozen Cu d states, computed with the Ceperley correlation. We see that freezing the d orbitals on Cu leads to a massive Cu d—Sep dehybridization, where the Cu d band separates from the upper valence band, forming a narrow isolated band at $E_{VBM} - 11.8$ eV. The dehybridization is accompanied by an opening of the fundamental band gap by 0.73 eV. We denote this d-orbital hybridization contribution to the band-gap anomaly by ΔE_g^d. If, instead of using the experimental anion displacement $u = 0.224$, we use the equal-bond structure with $u = \frac{1}{4}$, the effect of freezing the d orbitals (using Ceperley's correlation) is very similar: $\Delta E_g^d = 0.71$ eV. The consequences of the Cu d—Sep dehybridization on the bonding charge densities can be appreciated from Fig. 7. It compares the charge density at the top of the valence band after [Fig. 7(a)] and before [Fig. 7(b)] freezing the Cu d orbitals. It is seen that the nonzero covalent bond charge on the Cu—Se contact [Fig. 7(b)] vanishes upon freezing the Cu d orbitals [Fig. 7(a)] leading, therefore, to an enhanced ionic polarization of the bond charge. The Cu d character (fraction of d charge in this state within an atomic sphere around Cu) at the top
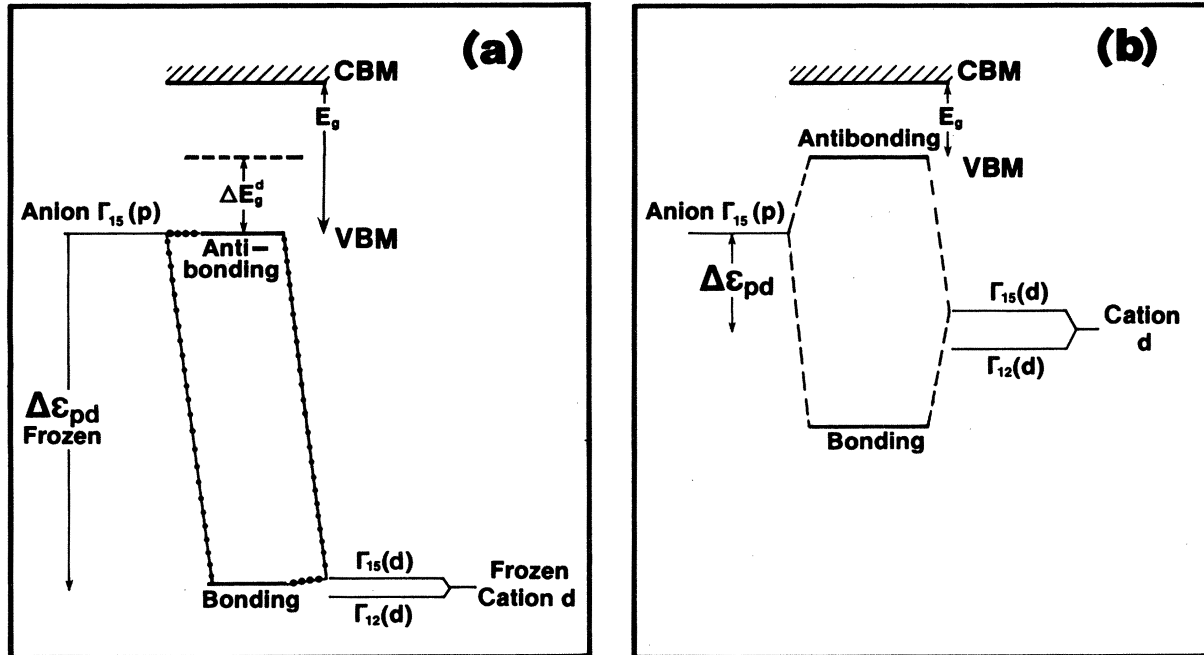
FIG. 8. Schematic molecular-orbital diagram used to discuss cation d-orbital effects on both the band-gap anomaly and acceptor binding energies. (a) Deep d orbitals, and (b) shallow d orbitals. See text for details.

of the valence band (the Γ_{4v} state) is reduced by 10% upon freezing the Cu d orbitals. We find very similar changes in the charge density at the conduction-band minimum upon freezing the Cu d orbitals.

The d-hybridization contribution ΔE_g^d to the band-gap anomaly has a simple molecular-orbital interpretation (Fig. 8). The outer valence p orbitals on the anion form, in a cubic field, a threefold-degenerate state, $\Gamma_{15}(p)$. The fivefold-degenerate d orbitals on the cation (separated by an energy $\Delta\epsilon_{pd}$ from the anion p states) transform in a cubic field into a threefold-degenerate $\Gamma_{15}(d)$ combination (with orbital lobes pointing and overlapping with the nearest-neighbor anions) and into a twofold-degenerate $\Gamma_{12}(d)$ combination (with lobes pointing between the nearest-neighbor anions, towards the next-nearest shell). (The Γ_{15} states can split further due to spin-orbit interactions into Γ_8 and Γ_7, and the doubly degenerate Γ_8 representation can split into $\Gamma_6+\Gamma_7$ in a noncubic field, but we will not consider these splittings in our simple argument here.) The states of the same symmetry $\Gamma_{15}(p)$ and $\Gamma_{15}(d)$ can interact, forming a lower bonding state [weighted more by the lower-energy $\Gamma_{15}(d)$ state] and an upper anti-bonding state [weighted more by a higher-energy $\Gamma_{15}(p)$ state]. The $\Gamma_{12}(d)$ states do not form any σ bonds with the nearest-neighbor atoms (although they do, however, form weaker π bonds). Perturbation theory[7] suggests that the two states, $\Gamma_{15}(p)$ and $\Gamma_{15}(d)$, will repel each other by an amount inversely proportional to $\Delta\epsilon_{pd}$ and directly proportional to the p-d coupling matrix element $|\langle p\,|\,V\,|\,d\rangle|^2$. In binary semiconductors such as GaAs, where the cation has only deep, corelike d states [or in CuBC_2 compounds with frozen Cu $3d$ orbitals; see Fig. 8(a)], the separation $\Delta\epsilon_{pd}$ is large and the direct p-d orbital overlap is very small due to the compactness of the cation

state. This leads to a small $\Gamma_{15}(p)$-$\Gamma_{15}(d)$ repulsion, and to an essentially pure cation d bonding states and a pure anion p antibonding state which forms the VBM. However, when the cation supports valence d states (e.g., Cu or transition atoms) the energy denominator $\Delta\epsilon_{pd}$ becomes small [Fig. 8(b)] and the cation d orbitals are more diffuse, overlapping more effectively with the anion orbitals. This leads to a substantial upward repulsion of $\Gamma_{15}(p)$ and a reduction $\Delta E_g^d \approx |\langle p\,|\,V\,|\,d\rangle|^2/\Delta\epsilon_{pd}$ in the band gap. The bonding combination results in a sharp Cu d—like resonance in the valence band (Fig. 4) and the antibonding combination forms the VBM (their separation is 3–4 eV in our calculation). Similar arguments will hold in the presence of the noncubic chalcopyrite crystal field. Hence, ΔE_g^d reflects a p-d hybridization effect.

This analysis suggests that only the p-d hybridization part ΔE_g^d of the total band-gap anomaly ΔE_g will correlate with the percentage of d character, and not the full anomaly ΔE_g, as suggested by Shay and Kasper.[55] This resolves the inconsistency encountered by Shay and Kasper for CuAlS$_2$. In Sec. V we will calculate the structural contribution ΔE_g^S to the band-gap anomaly. We will show that the chemical contribution, defined as the difference between the total ΔE_g and ΔE_g^S, does in fact scale linearly with the percentage of d character calculated from the wave function, and that CuAlS$_2$ is no exception.

Before closing our discussion on the p-d hybridization, we point to an interesting analogy in impurity physics. It has been known for a long time (e.g., review in Ref. 56) that whereas III-V and IV-IV semiconductors can be made low-resistivity p-type semiconductors by substitutions of impurity atoms with one less valence electron on the cation site (e.g., Zn in GaAs or Ga in Si), the same is not true for II-VI compounds. Doping of ZnS or ZnSe by
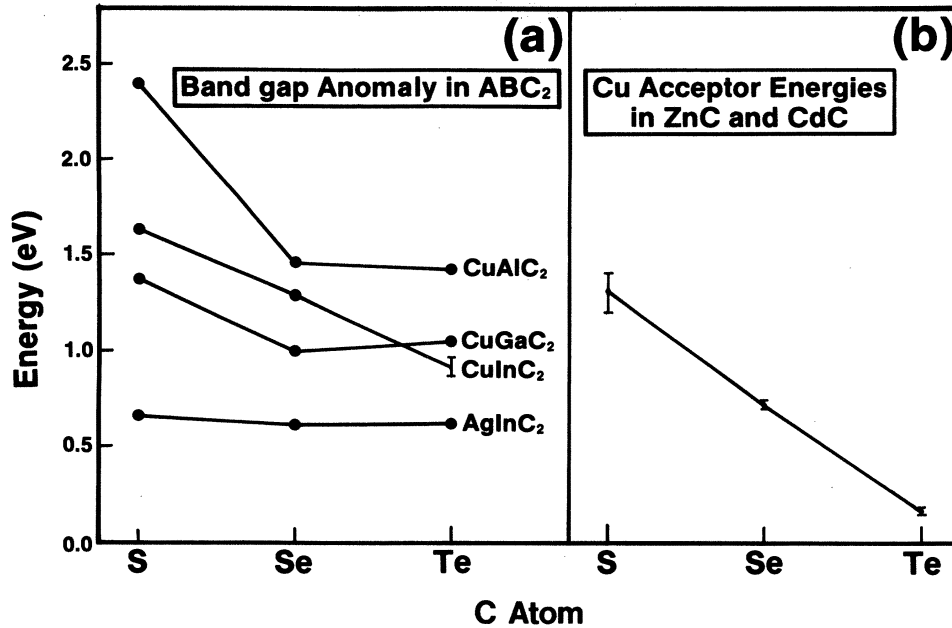
FIG. 9. Variation of (a) the band-gap anomaly in $CuBC_2$ chalcopyrites, and (b) Cu acceptor binding energies in II-VI compounds (Refs. 56 and 57), with the position of the anion in the Periodic Table.

Cu is thought to lead (aside from interstitials, Cu precipitates and various Cu sulphides) also to Zn substitutions. However, instead of leading to shallow states, this leads to *deep* acceptors, about 1.4 and 0.7 eV above the VBM, respectively.[56,57] We suggest that the *p-d* hybridization contribution to the reduction of the band gaps in ternary chalcopyrites and the anomalously deep Cu acceptors in II-VI compounds share a common physical origin: Both result from the existence of a small $\Delta\epsilon_{pd}$ energy separation (i.e., Cu *d* to anion *p*) which repels the antibonding state upwards. This antibonding state is the VBM in ternary chalcopyrites and the acceptor level in Cu impurities in II-VI compounds. Indeed, the Cu acceptor energies in II-VI compounds *decrease* with $\Delta\epsilon_{pd}$ (in the sequence ZnS→ZnSe→ZnTe the anion binding energy decreases, and consequently, the acceptor energy decreases from 1.4 to 0.7 and 0.14 eV, respectively), whereas the cation has little influence on the acceptor energies (ZnX and CdX having very similar Cu acceptor energies). This is illustrated in Fig. 9. In contrast, doping II-VI materials by Na that lacks *d* orbitals usually results in shallower acceptors of energy,[56] ≤ 0.1 eV (the material shows, however, high *p*-type resistivity due to donor-acceptor compensation).

IV. CATION-ELECTRONEGATIVITY FACTOR

The virtual process of bringing a chalcopyrite compound into *chemical* analogy with a zinc-blende compound consists of two steps. (i) Freeze the *d* orbitals on the Cu atom. The resulting contribution to the band-gap anomaly is the *p-d*—hybridization part

$$\Delta E_g^d = E_g(ABC_2, \text{frozen } d) - E_g(ABC_2, \text{active } d)$$

discussed in the preceding section. (ii) With the use of the

frozen *d* structure, replace the two cations by the average cation. The resulting contribution to the band-gap anomaly is referred to as cation electronegativity (CE) and is given by

$$\Delta E_g^{CE} = E_g(\langle AB \rangle C_2, \text{frozen } d) - E_g(ABC_2, \text{frozen } d),$$

where $\langle AB \rangle$ denotes the average cation. For example, since the Zn atom is situated in the Periodic Table between Cu and Ga, the CE contribution to the band-gap anomaly of $CuGaS_2$ is the difference in the band gap of $ZnZnS_2$ (ZnS in a chalcopyrite lattice) and $CuGaS_2$, both with frozen *d* orbitals. The CE term reflects the fact that in a chalcopyrite structure, even if the *d* electrons were chemically inactive, charge could separate differently on the two dissimilar cations, thereby affecting the band gap. In ternary chalcopyrites, the CE contributions to ΔE_g ($\sim$0.1–0.2 eV) are found to be considerably smaller than the *p-d* hybridization contribution ΔE_g^d and the structural contribution ΔE_g^S discussed in Sec. V. In ternary pnictides (e.g., $ZnSiP_2$) and in alloys of III-V compounds[58] (e.g., InP-GaP), where $\Delta E_g^d \simeq 0$, the CE contribution is not negligible, as was shown before.[58] Electrostatically, this means that when the valence charge $\bar{Z}$ on the zinc-blende cation is separated into $Z_A = \bar{Z} - 1$ and $Z_B = \bar{Z} + 1$ in the chalcopyrite structure, the valence electrons will attempt to screen these point-ion perturbations, resulting in a lower bond charge on A—C and a higher bond charge on B—C. Clearly, the lattice is no longer in equilibrium with this new charge distributions. The system will respond by moving the atoms to new equilibrium positions, resulting in $R_{AC} \neq R_{BC}$. As a result, more charge will be placed on the shorter bond (Cu—Se) and less charge will reside on the longer bond (In—Se). This simple electrostatic picture is explained in the light of our detailed calculations in the following section.
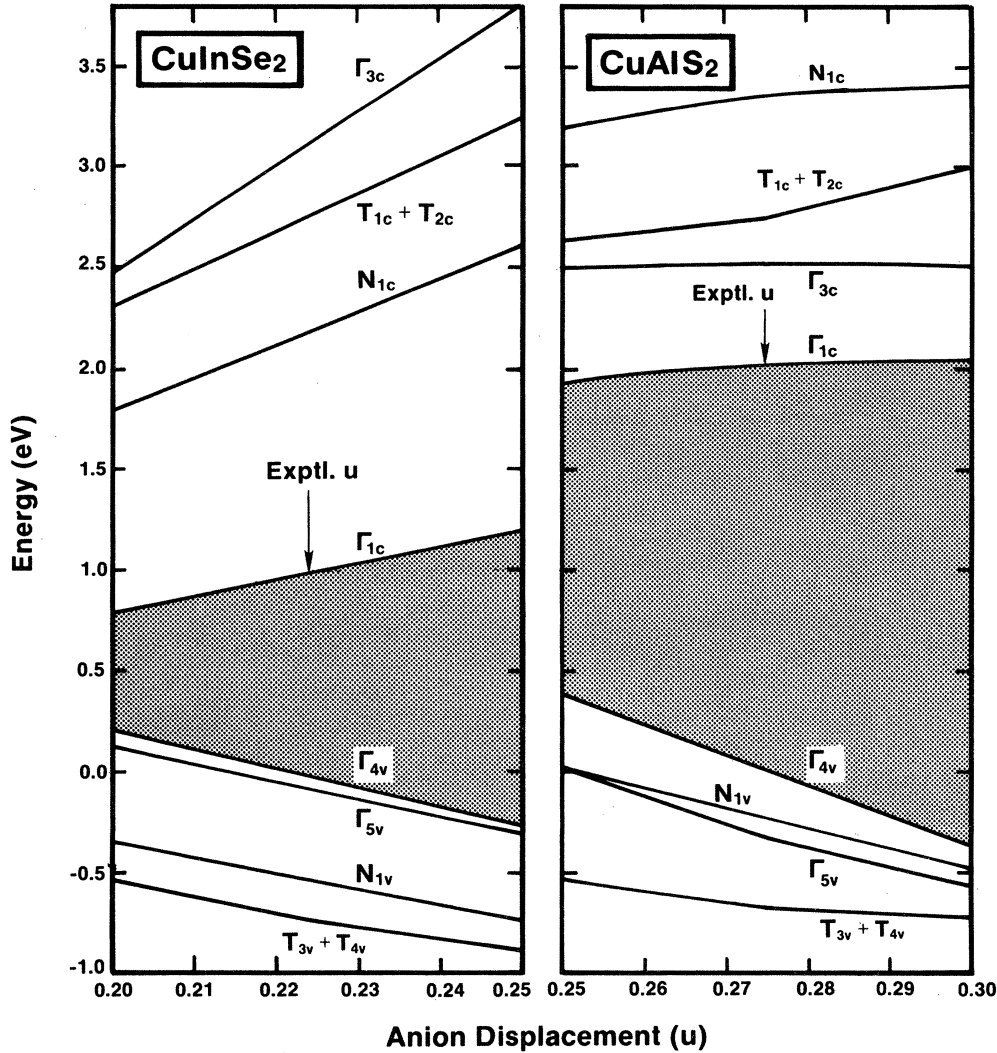
FIG. 10. Variation of band energies at high-symmetry points for CuInSe$_2$ and CuAlS$_2$ with the anion displacement parameter u. The results for CuInSe$_2$ are calculated with Slater-type exchange, whereas those for CuAlS$_2$ (which has a nonvanishing gap even with Ceperley's correlation) are calculated with Ceperley's correlation. Shaded areas denote the direct band gap; horizontal arrows point to the experimental equilibrium u values.

V. STRUCTURAL EFFECTS ON THE BAND GAP

The experimental data alone[55] suggest that p-d hybridization does not account for the full band-gap anomaly since compounds with similar d character[55] (e.g., CuAlSe$_2$ and CuGaSe$_2$) differ substantially in their band-gap anomaly. We suggest that this is due to a structural (S) anomaly relative to the binary analogs and denote the corresponding contribution to ΔE_g as ΔE_g^S.

We start by eliminating another possibility, namely that the existence of a tetragonal deformation $\eta \equiv c/2a \neq 1$ controls E_g. Calculation of the CuInSe$_2$ band structure as a function of η indicates that the band gap changes by less than 0.05 eV when η is varied between[28] 1.000 and 1.004 and only the crystal-field splitting (separation between the two upper valence-band states Γ_{4v} and Γ_{5v}) changes with η (nearly linearly). [In ternary pnictides, e.g., ZnSiP$_2$, where η is usually considerably smaller than 1 (cf. Table II), increasing η to 1.0 reduces the band gap by $\sim 10\%$.]

The next possibility we examine is the role of the

nonideal anion displacements $u \neq \frac{1}{4}$. We note at the outset that bond alternation in itself could not explain ΔE_g since, for example, CuGaSe$_2$ shows no bond alternation but still has a substantial ΔE_g. In such cases we find (cf. Sec. VI) that the chemical effect alone (Sec. III) explains ΔE_g. To study the contributions of the structural effects, we first note that Eq. (1) shows that variation of u compresses one anion—cation bond and dilates the other according to $u - \frac{1}{4} = \alpha/a^2$, where $\alpha = R_{AC}^2 - R_{BC}^2$ is the bond-alternation parameter. We have performed self-consistent band-structure calculations for a number of chalcopyrites as a function of u, keeping the unit-cell dimensions constant ($a = a_{\text{expt}}$ and $\eta = \eta_{\text{expt}}$). Figure 10 displays the variations of the energies of a few-symmetry states below and above the VBM in CuInSe$_2$ and CuAlS$_2$ with u. The experimental equilibrium value of u is indicated by the vertical arrows.

We find that the valence-band states drop in energy with increasing u while the conduction-band states rise with u. While the slope differs for the various states, the

lowest direct ($\Gamma\Gamma^*$, NN^*, and TT^*) and indirect (ΓN^*) gaps vary with a similar slope (Fig. 11), with $\partial\Delta\epsilon/\partial u$ in the range of 19—22 eV. In particular, the first band gap of CuInSe$_2$ increases by $\Delta E_g^S = 0.47$ eV when u is varied from its equilibrium value of 0.224 to its ideal zinc-blende value, $u = \frac{1}{4}$, complementing the chemical contribution $\Delta E_g^d = 0.73$ eV to a total of $\Delta E_g = \Delta E_g^d + \Delta E_g^S = 1.2$ eV, close to the experimental band-gap anomaly of 1.3 eV. In other words, setting $u = 0.25$ *and* freezing the d orbitals gives for CuInSe$_2$ almost the same band gap as its binary analog. We shall see in Sec. VI that the same is true for CuAlS$_2$, where ΔE_g^d is much larger.

To study the mechanism of structurally induced gap variations, we consider in Fig. 12 the changes in the charge densities at the top of the valence band of CuInSe$_2$ with u. The solid lines denote the charge densities for $u \neq \frac{1}{4}$, whereas the dashed lines give, for comparison, the results for the equal-bond arrangement $u = \frac{1}{4}$ (relative to the anion site as origin). We see that as u increases from 0.20 through the equilibrium value of 0.224 to $u = 0.25$, the Cu—Se bond charge decreases while the In—Se bond charge increases, weakening and strengthening the two bonds, respectively. This trend parallels the changes in the bond lengths: Upon increasing u, the Cu—Se bond length increases, whereas the In—Se bond length decreases. Clearly, as the top of the valence band is weighted more heavily by Cu—Se contributions,[58] the reduction in the covalency of this bond upon increasing u to its ideal zinc-blende value opens up to the band gap. The anion displacement u controls, therefore, the balance between the ionic and covalent contributions to the band gap, increasing the former at the expense of the latter (and increasing the total band gap) as u increases. The effect of u on the *total* valence-band charge density is seen in Fig. 13, where the same contours around the Cu—Se bonds are
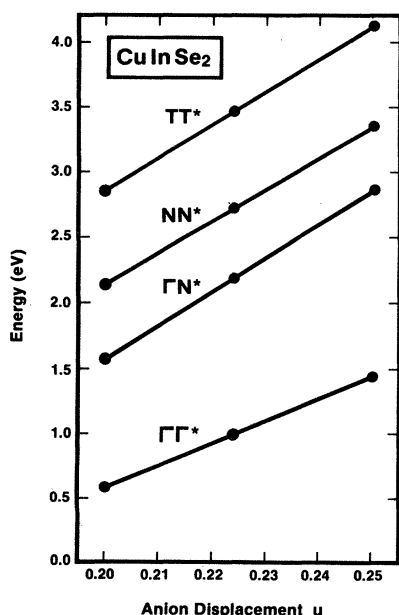
shaded to highlight the disengagement of the Cu—Se bond upon the formation of the more ionic zinc-blende-like equal-bond structure. The conduction-band minimum (CBM) responds in an opposite way to the VBM: As u increases, its energy rises as *more* bond charge is placed on this strongly antibonding Cu—Se state. The structurally induced changes in the atomic character of various band states can be seen in Fig. 14, depicting the breakdown of the total charge in a state $|i\rangle$ into its atom (γ) centered contributions $Q_\gamma[i]$. (Notice that these charges are calculated from the Slater-exchange band structure and hence are not expected to be as accurate as those calculated with Ceperley's correlation; we use the former charges only to discuss changes with u.) We see that the VBM (Γ_{4v} state) is weighted more heavily by Cu-Se contributions, and as u increases from 0.20 to 0.25 the Cu content decreases and the Se content increases, thereby reducing the p-d hybridization. In contrast, the CBM (Γ_{1c} state) is weighted more heavily by the cation having less tightly bound valence electrons (In), and hence, constitutes an In-Se state. As u increases, the In contribution to the CBM rises and the Se contribution decreases, leading to a destabilization of this state and an increase in its energy.

The general trend that we find in a number of materials is similar: The conduction band is lowered as the bond that contributes the most to it (involving the cation with less-bound outer electrons, e.g., In s rather than Cu d) is stretched. For example, as u decreases in CuInSe$_2$, the In—Se bond making up the CBM is stretched; in the fictitious compound GaInP$_2$ the In—P bond making up the CBM is stretched as u increases, etc. In both cases, the CBM is lowered in energy. On the other hand, the VBM is raising in energy as the bond contributing the most to it (involving the cation with the tighter bound outer electrons, e.g., Cu d rather than In s) is compressed. For example, as u is decreased in CuInSe$_2$, the Cu—Se bond making up the VBM is compressed, raising the energy of the VBM. We conclude that the structurally induced variations in the band gaps are a consequence of the *internal stress* exerted by compression and stretching of the bonds that contribute mostly to the wave functions of the VBM and CBM. The internal stress induced by bond alternation has a significant consequence on the hybridization. In the ideal zinc-blende structure where the atoms are at tetrahedral sites, the Γ_{25} representations (e.g., the VBM) cannot mix s character, whereas the Γ_1 representations (e.g., the CBM) cannot mix p or d character. As the anions are displaced, this is no longer true, and the zinc-blende VBM and CBM states can admix in forming the chalcopyrite band edges. It is this s-p-d hybridization that leads to the reduction in the band gap upon anion displacement. Clearly, higher-energy gaps or indirect gaps (which are already sp hybrides in the zinc-blende structure) will be affected to a lesser extent.

We wish to point to an interesting analogy between the structural contribution ΔE_g^S to the chalcopyrite band-gap anomaly and the optical bowing in semiconductor alloys.[58] It is well known [e.g., reviews in Refs. 59(a)—59(c)] that the lowest band gaps of semiconductor alloys are usually smaller than the concentration- (x-) weighted average of the band gaps of the constituent binary semiconductors.

FIG. 11. Variation of the lowest direct ($\Gamma\Gamma^*$, NN^*, and TT^*) and indirect (ΓN^*) band gaps of CuInSe$_2$ with the anion displacement u.

FIG. 12. Effect of varying the anion displacement parameter u on the charge density at the VBM in $CuInSe_2$. (a) $u = 0.20$, (b) $u = 0.224$ (equilibrium value), and (c) $u = 0.25$ (ideal zinc-blende value). The dashed lines denote, for comparison, the bond-charge (with respect to Se as origin) for the equal-bond ideal zinc-blende arrangement. ΔQ denotes the change in the Cu d character relative to the equilibrium structure. Note that increasing u lowers the charge on the stretched Cu—Se bond (reducing its Cu d character), and raises the charge on the compressed In—Se bond, weakening and strengthening these two bonds, respectively.

FIG. 13. Logarithmically spaced contour plots of the total valence-band (VB) charge density of $CuInSe_2$ for two values of the anion displacement parameters, indicating the disengagement of the covalent Cu—Se bond charge (shaded areas) upon increasing u to form an equal-bond zinc-blende-like arrangement ($u = 0.25$).

Anion Displacement (u)

FIG. 14. Variation of the band charges [charge due to a given band enclosed in spheres of atomic radii (Ref. 26)] with the anion displacement u in $CuInSe_2$. The solid lines represent charges at the VBM (the Γ_{4v} state), whereas dashed lines denote charges at the CBM (the Γ_{1c} state). The difference between $Q_{Cu}+Q_{Se}+Q_{In}$ and 100% is due to the charge outside atomic spheres. Values are calculated from the Slater-type—exchange band structure and are hence only qualitative. Notice that upon increasing u, the Cu charge diminishes at the VBM, whereas the In charge increases at the CBM, leading to a decrease (increase) in the energies of the VBM (CBM), and hence an increase in the band gap.

This alloy band-gap reduction ΔE_g^{alloy} is often expressed phenomenologically by the relation $\Delta E_g^{alloy} \equiv bx(x-1)$, where the bowing parameter $b>0$ reflects an upward concave nonlinearity in $E_g(x)$. We have pointed out[58] that a large fraction of b can be explained by considering the fact that such alloys do not have a single (average) cation-anion bond length, but instead, as discovered by Mikkelson and Boyce,[60] can be thought of as having a local chalcopyrite coordination with a bond alternation $\alpha = R_{AC}^2 - R_{BC}^2$ and anion displacement $u - \frac{1}{4} = \alpha/a^2 \neq 0$. For an equimolar composition of GaP and InP we calculate[58] an equilibrium value of $u = 0.278$. Using this result, we can now calculate the structural contribution to ΔE_g^{alloy} by comparing the band gaps of an equal-bond compound InGaP$_2$ ($u = \frac{1}{4}$) with that of a similar compound but with bond alternation ($u = 0.278$). We find that upon increasing u from $u = \frac{1}{4}$ (i.e., stretching the In—P bond), the CBM made up predominantly from In-P contributions (In has a smaller binding energy than Ga) is lowered, thereby reducing the band gap. The amount of this band-gap lowering (proportional to the sp mixing of the band edges induced by bond alternation) explains most of the observed optical bowing in equimolar InP-GaP alloys.[58,59]

Bond Length Mismatch $\alpha = R_>^2 - R_<^2$ (a.u.)
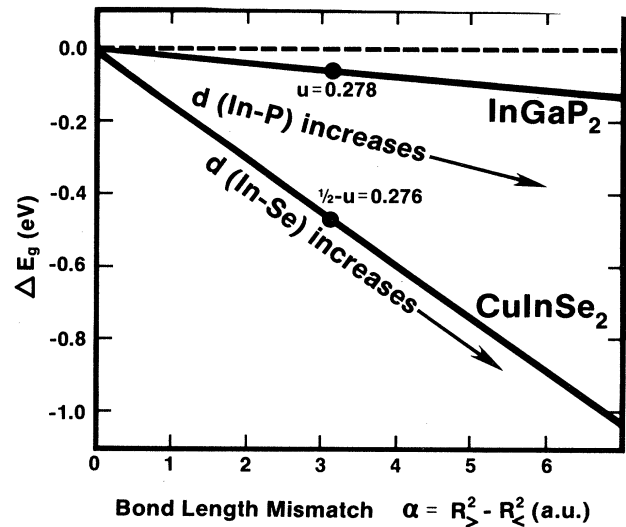
FIG. 15. Comparison between the structurally induced reduction in the band gaps of the fictitious InGaP$_2$ chalcopyrite crystal and CuInSe$_2$. The solid circles denote the equilibrium values of u (in InGaP$_2$) and $\frac{1}{2}-u$ (in CuInSe$_2$). As the bond contributing mostly to the CBM (In—P and In—Se) is stretched (corresponding to an increase of u in InGaP$_2$ and a decrease in u CuInSe$_2$), the CBM is lowered and the band gap is reduced. The structurally induced band-gap has the same physical origin in both classes of compounds, the only difference being the magnitude of the effect. (Note that this definition of the structural parameter α differs slightly from that given in the text in Sec. VII.)

The common origin of the ΔE_g^S effect in chalcopyrites and the ΔE_g^{alloy} effect in alloys is illustrated in Fig. 15. In InGaP$_2$, an increase of u corresponds to stretching the In—P bond, whereas in CuInSe$_2$ an increase in $\frac{1}{2}-u$ corresponds to a stretching of the In—Se bond. In both cases the band gap decreases, primarily due to the lowering of the CBM. The difference between the band-gap anomaly in CuInSe$_2$ and the alloy bowing in InGaP$_2$ is largely quantitative: While in CuInSe$_2$ the gap decreases with $\partial E_g/\partial(\frac{1}{2}-u)=18$ eV, in InGaP$_2$ the derivative is far smaller, $\partial E_g/\partial u = 1.5$ eV, due to the smaller electronegativity differences of the constituent atoms. This analogy suggests to us that under careful alloy growth conditions it may be possible to produce new (metastable) phases of alloys $A_x B_{1-x} C$ having a chalcopyrite-like ordering, if the alloyed elements (e.g., A and B) are sufficiently different.

VI. DISCUSSION OF THE TOTAL BAND GAP ANOMALY

We have shown that the band-gap anomaly can be analyzed in terms of a chemical factor ΔE_g^{chem} and a structural factor ΔE_g^S. The chemical factor consists of a p-d hybridization effect ΔE_g^d and a cation electronegativity effect ΔE_g^{CE} where the former is dominant in Cu chalcopyrites and the latter is dominant in Zn and Cd pnictides or in alloys of binary semiconductors, e.g., GaAs-InAs. The structural contribution to the band-gap anomaly ΔE_g^S has a smaller contribution due to variations in the

TABLE III. Decomposition of the observed band-gap anomaly (cf. Table I) into its calculated structural component ΔE_g^S and chemical component ΔE_g^{chem}. The major contribution to the latter is seen to arise from the d-hybridization effect (ΔE_g^d) calculated for the two end compounds. For comparison, we give the value of the experimental anion displacement (Ref. 28) and the calculated percentage of d character at the top of the valence band (using Ceperley's correlation at the observed value of the anion displacement; cf. Fig. 16).

Material	ΔE_g^{obs}	u	ΔE_g^S	$\Delta E_g^{chem} \equiv \Delta E_g^{obs} - \Delta E_g^S$	ΔE_g^d	α_d (%)
$CuInSe_2$	1.3	0.224	0.5	0.70	0.72	22
$CuInS_2$	1.6	0.214	0.7	0.9		24
$CuGaSe_2$	1.0	0.25	0.0	1.0		25.1
$CuAlSe_2$	1.4	0.269	−0.38	1.81		27.5
$CuGaS_2$	1.4	0.275	−0.50	1.87		31.5
$CuAlS_2$	2.4	0.275	−0.50	2.90	2.98	35.2

tetragonal strain ($\eta \neq 1$), and a larger contribution due to bond alternation ($\alpha \neq 0$ or $u \neq \frac{1}{4}$). Denoting $\Delta = u - \frac{1}{4}$, we can treat Δ as the small parameter of the problem and describe the structural part of the band-gap anomaly by retaining two powers of Δ, i.e., $\Delta E_g^S \simeq a\Delta + b\Delta^2$. Clearly $a = 0$ when the two cations A and B are equal, since the transformation $\Delta \rightarrow -\Delta$ then carries the lattice into itself. This suggests that the linear structural effect $a\Delta$ depends primarily on the chemical *difference* between the cations. The electronegativity difference between A and B may hence be thought of as a reasonable measure of the coefficient a. Indeed, we find in our calculation a large structural derivative (18–21 eV) for Cu chalcopyrites (e.g., 18.2 eV for $CuInSe_2$ with a $Cu-In$ electronegativity difference of 0.2, and 20 eV for $CuAlS_2$ with a $Cu-Al$ electronegativity difference of 0.4) and a far smaller structural derivative for the fictitious III-III-V_2 chalcopyrites (e.g., 1.5 eV for $InGaP_2$ with a small $In-Ga$ electronegativity difference). Note that the nonlinear structural term $b\Delta^2$ need not vanish for the zinc-blende structure (i.e., variations of the two bonds Zn_a-S and Zn_b-S in a $Zn_a Zn_b S_2$ structure can change the band gap symmetrically with Δ). In systems with chemically similar cations (i.e., alloys such as GaP-InP), this nonlinear term (proportional to the *average* electronegativity, rather than the electronegativity difference, and hence similar in binary and ternary materials) is likely to be the dominant effect. We conclude that the band-gap anomaly in Cu chalcopyrites is controlled by ΔE_g^d and $\Delta E_g^S \simeq a\Delta$, and that the optical bowing in semiconductor alloys is controlled by ΔE_g^{CE} and $\Delta E_g^S \simeq b\Delta^2$. This is consistent with the discovery[59(c)] of a remarkably successful linear scaling between the optical bowing parameter of In-Ga-As-P alloys and the electronegativity difference of the substituted elements. We see, however, that the existence of such a scaling need not indicate the predominance of disorder effects,[59(a)] but rather, it merely suggests that $\Delta E_g^{alloy} \cong \Delta E_g^{CE}$ when structural distortions are small. ΔE^{CE}, in turn, exists already in ordered systems. In ternary pnictides it is likely that the band-gap anomaly is controlled by both ΔE_g^{CE} and $\Delta E_g^S = a\Delta + b\Delta^2$.

In Table III we have decomposed the observed band-gap anomalies of Cu chalcopyrites into a structural part ΔE_g^S calculated from our u variation of the band gaps, and into a chemical part defined here as the difference $\Delta E_g^{chem} \equiv \Delta E_g - \Delta E_g^S$. We note the following. (i) Bond

alternation is responsible for *reducing* the band gap of $CuInS_2$ and $CuInSe_2$ relative to their binary analogs, while in $CuAlS_2$, $CuAlSe_2$, and $CuGaS_2$ bond alternation *increases* the gap relative to the corresponding binary analogs, consistent with $\Delta = u - \frac{1}{4}$ being negative for the first group and positive for the second group. (ii) The chemical contribution leads uniformly to a reduction in the band gaps. (iii) For the two "end compounds" for which we have calculated the p-d hybridization component of the chemical shift, we find that ΔE_g^{chem} and ΔE_g^d are very close, confirming the relative unimportance of CE effects in these compounds. (iv) The calculated d character of the wave functions at the top of the valence band (denoted α_d; we calculate it using the Ceperley correlation at the equilibrium anion displacement since this correlation produces better agreement[26] with the position of the d states observed in photoemission) is proportional to the chemical shift (Fig. 16). In contrast to the Shay-Kasper correlation of the *total* band-gap anomaly ΔE_g with the empirically determined d character, $CuAlS_2$ is no exception to our rule. The reduction of the spin-orbit splitting in the ternary compounds relative to the binary compounds forms an (admittedly crude) spectroscopic measure (observable) to ΔE_g^d.

VII. ANALYSIS OF STRUCTURAL PARAMETERS IN TERMS OF ELEMENTAL COORDINATES

Having established the influence of anion displacements on the structural part of the band-gap anomaly in ternary chalcopyrites, we turn to the question of what controls the anion displacements. We give in the first five columns of Table II a compilation of the measured lattice parameters and anion displacements of ternary chalcopyrites and pnictides (note that u is not measured directly, but rather is obtained in a crystallographic structural refinement that is sensitive to the assumed atomic structure factors, anisotropic temperature coefficients, dispersion corrections, and method of performing best-fit analysis). Despite the substantial scatter in results for the same materials, significant material dependence of u is evident from Table II. A superficial inspection of these trends show that they do not follow any simple chemical rules. While a quantum-mechanical minimization of the total energy $E(a,\eta,u)$ would certainly be desirable for determining the predicted structural parameters, we first wish to organize this rather
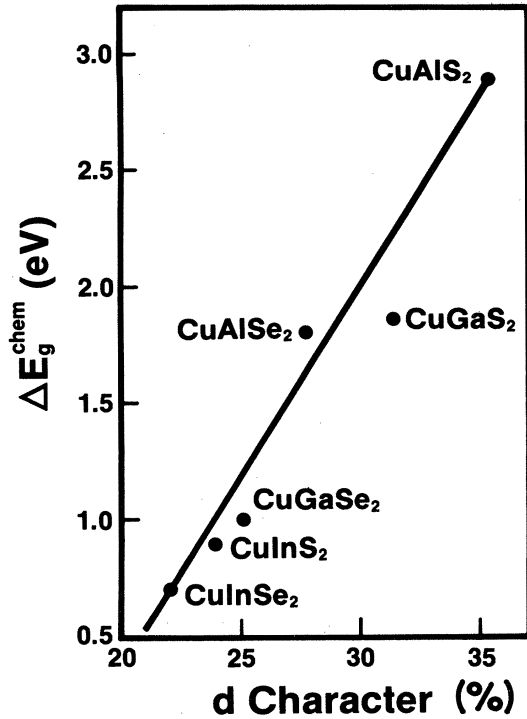
FIG. 16. Correlation between the chemical contribution to the band-gap anomaly and the percentage of d character of the top of the valence band, calculated from the Ceperley-correlation band structures of six Cu-based chalcopyrites.

chaotic data base in terms of elemental properties[24] to unravel the underlying chemical trends. This may be helpful not only for obtaining the u parameters for compounds for which they were not measured (e.g., II-IV-Sb$_2$ compounds), but also for being able to control u artificially by chemical means, and hence design compounds with desired band gaps.

Considerable attention has been focused in the past on the systematization of the values of the tetragonal distortion parameter η. Since these have only little importance for controlling the band gaps, we will mention these ideas only in passing. Folberth and Pfister[61] suggested that $1-\eta$ is related to the polarization of the $A-C$ and $B-C$ bonds, and should therefore be proportional to the difference $(r_A/r_B)_{\text{covalent}}-(r_A/r_B)_{\text{ionic}}$, where r_A and r_B are the corresponding covalent and ionic radii. The correlation obtained was only qualitative. Phillips[62] worked out a phenomenological fit of $2(1-\eta)$ to a linear combination of elemental dielectric electronegativities which worked fairly well for II-IV-V$_2$ compounds with small distortions but not for those with large distortions. Chelikowsky and Phillips[63] later developed a theory of empirical atomic orbital radii and applied it to the chalcopyrite tetragonal distortion; they found an empirical formula that gave a good fit for all the II-IV-V$_2$ compounds except CdSnP$_2$ and CdSnAs$_2$. The physical significance of the fitting parameters remains, however, elusive. A similar study was reported by Shaukat and Singh,[64] (although it can be
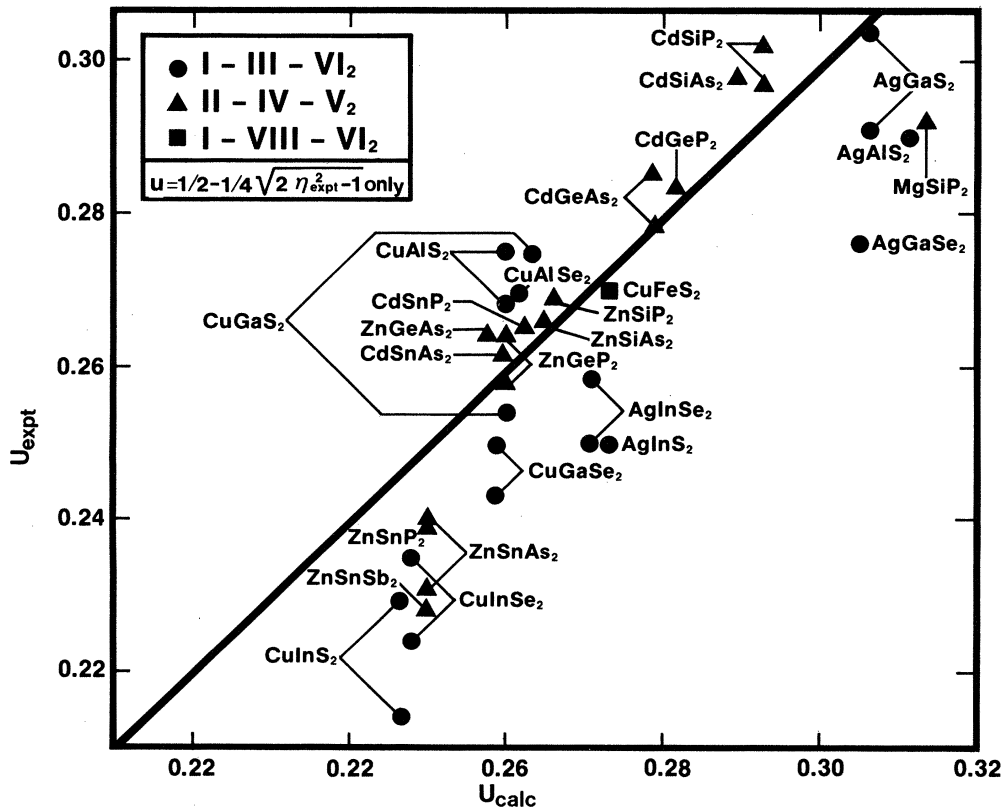
FIG. 17. Predictions of anion displacement parameters u from the simple tetrahedral rule [Eq. (3)]. Data for u from Hahn et al. (Ref. 27) are excluded since they conflict with all other available measurements. Multiple arrows denote different experimental determinations (cf. Table II). Poor correlation is obtained for $A\,\text{In}C_2$, $Ag BC_2$, and $ZnSnC_2$ compounds.

dramatically improved; cf. Ref. 64), whereas Noolandi[65] developed a consistent force-field model for tetragonal distortions. The systematization of the anion displacement parameters u has received much less attention,[24,41] and no work exists, to our knowledge, on the systematization of the lattice parameters a.

Abrahams and Bernstein[30] have proposed that the bond angles at the B atom in ABC_2 chalcopyrites would have the ideal tetrahedral (tet) values, which would require that u and η be related by

$$u = u_{\text{tet}}(\eta) = \tfrac{1}{2} - \tfrac{1}{4}(2\eta^2 - 1)^{1/2} . \tag{3}$$

The experimental values of η were then used to predict u. The results of this correlation (including more compounds than in Ref. 30) are displayed in Fig. 17; the model gives good agreement for the II-IV-V$_2$ compounds (as noted by Abrahams and Bernstein) when the column-IV atom was Si or Ge, but much worse results were obtained for II-Sn-V$_2$ compounds (where the tendency towards metallicity of Sn makes it possible to accommodate nontetrahedral bonds around it) and for most I-III-VI$_2$ compounds (as seen in our Fig. 17). Improved agreement was obtained by fitting the deviation from Eq. (3) to a linear combination of atomic electronegativity with statistically fitted numerical coefficients,[30,32] especially if different coefficients were used for I-III-VI$_2$ and II-IV-V$_2$ compounds; however, this improvement comes at the cost of using a purely ad hoc numerical fit with little physical motivation. More recently, DeGil[66] derived limiting inequalities for the chalcopyrite structural parameters, while correlations among their temperature derivatives were studied by Bhar and Samanta.[67]

Our own approach to the problem is inspired by Bragg's[68] classical principle of transferability and conservation of elementary bonds in different compounds. An enormous body of crystallographic studies has been directed at defining elemental radii that add up to produce the measured bond length $R_{ij} \simeq r_i + r_j$. Surprisingly, however, this idea has received only a little attention for the ternary ABC_2 compounds. Pfister[47] used a simple scheme based on atomic radii to estimate u for a few II-IV-V$_2$ compounds, while Chemla et al.[69] developed a scheme combining atomic radii with an approach similar to that of Abrahams and Bernstein.[30,32] Working to lowest order in $1 - \eta$ and $u - \tfrac{1}{4}$, and assuming a relation equivalent to (3), they used bond-length considerations to predict both u and η, and then fitted the residual error in η to a simple function of the atomic electronegativity. As did other authors,[30,32] they too found poor agreement for ZnSnV$_2$ compounds, which they argued might not really have the chalcopyrite structure; they did not treat the I-III-VI$_2$ materials.

The ternaries not only offer a large data base (Table II) but also provide a more stringent test to the hypothesis that, to low order, the R_{A-C} bond lengths do not depend on the B atom, etc. Figure 18 shows the correlation between the observed bond lengths of ternary ABC_2 materials and the sum of Pauling's tetrahedral radii.[70] A somewhat better correlation can be obtained using the Shannon-Prewitt radii;[71] however, the latter are only available for a few of the bonds considered in Fig. 18. We see

that whereas the spread in R_{ij} for fixed i and j is certainly non-negligible (reflecting not only the experimental error, but also the significance of genuine chemical factors of nonpairwise additivity), the overall correlation is reasonable, highlighting the success of Bragg's idea (dating back to 1920!) which we refer to as the "conservation of tetrahedral bonds" (CTB). In light of the classical notion, the discovery by Mikkelsen and Boyce[60] of the conservation of the In—As and Ga—As bond lengths in an In$_x$Ga$_{1-x}$As alloy comes as no surprise. The implication of this principle for the structural parameters a, η, and u of ABC_2 compounds is that these degrees of freedom would attain values that minimize simultaneously the difference between the actual anion-cation bond lengths R_{AC} and R_{BC} and the sums of elemental radii,

$$R_{AC}(a,\eta,u) - r_A - r_C = 0 , \quad R_{BC}(a,\eta,u) - r_B - r_C = 0 . \tag{4}$$

For ternary chalcopyrites,

$$R_{AC}(a,\eta,u) = \left[u^2 + \frac{1+\eta^2}{16} \right]^{1/2} a ,$$

$$R_{BC}(a,\eta,u) = \left[(u - \tfrac{1}{2})^2 + \frac{1+\eta^2}{16} \right]^{1/2} a . \tag{5}$$
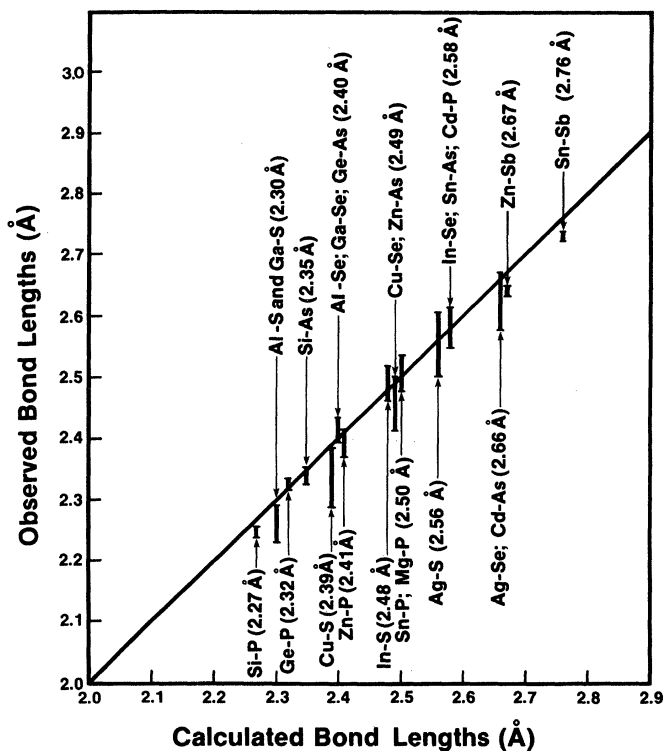
FIG. 18. Correlation between the observed bond distances (vertical axis; the range indicated covers all available data for the ternaries) and the sum of Pauling's tetrahedral radii (horizontal axis). Although the correlation can be improved by using the Shannon-Prewitt radii (cf. Table V), the correlation presented here already suggests that the global structural parameters of these compounds are dictated by the mismatch in local bonds. The spread of the data shown reflects experimental errors as well as the deviations from pairwise additivity of elemental radii.

Since Eqs. (4) can predict only two unknowns, a third condition is needed. This suggests two approaches.

A. CTB plus $\eta = \eta_{expt}$ rule

In the first approach, denoted "CTB plus $\eta = \eta_{expt}$ rule," we set the tetragonal distortion parameter equal to its experimental value and solve for a and u. This is based on the fact that Eqs. (4) and (5) show only a weak dependence of the bond lengths on η.

Defining the bond mismatch parameter as

$$\alpha = R_{AC}^2 - R_{BC}^2 = (r_A + r_C)^2 - (r_B + r_C)^2 , \tag{6}$$

and the mean-square bond as

$$\beta = R_{AC}^2 + R_{BC}^2 = (r_A + r_C)^2 + (r_B + r_C)^2 , \tag{7}$$

the solutions to Eqs. (4) are

$$a^2 = \frac{4\alpha^2}{\beta - [\beta^2 - (2 + \eta^2)\alpha^2]^{1/2}} ,$$

$$u = \frac{(\alpha + \beta) - [\beta^2 - (2 + \eta)^2\alpha^2]^{1/2}}{4\alpha} = \frac{1}{4} + \frac{\alpha}{a^2} . \tag{8}$$

Figure 19 displays the correlation between the calculated lattice parameter a [in Eq. (8)] and the observed one, whereas Fig. 20 gives a similar comparison for the anion displacements u. It is seen that this method gives excellent agreement for the lattice constant a and reasonable agreement for the anion displacement u (the latter being somewhat obscure by the large scatter in the experimental data). The agreement for u is, however, consistently better than that obtained by the Abrahams-Bernstein rule [Fig. 17 and Eq. (3)].

The structure of Eqs. (8) suggests expansion in terms of the small parameter $\delta \equiv \alpha/\beta$. This gives

$$a = \left[\frac{8\beta}{2 + \eta^2} \right]^{1/2} \left[1 - \frac{2 + \eta^2}{8}\delta^2 + O(\delta^4) \right] ,$$

$$u = \frac{1}{4} + \frac{2 + \eta^2}{8}\delta + \frac{2 + \eta^2}{32}\delta^3 + O(\delta^5) . \tag{9}$$

Recalling that the zinc-blende (ZB) lattice constant is given as $a_{ZB} = \frac{1}{2}(\frac{16}{3})^{1/2}R_{AC}$, we see from Eqs. (9) that the correction for $a - a_{ZB}$ is *second* order in δ (for $\eta = 1$), whereas the correction for $u - \frac{1}{4}$ is already *first* order in
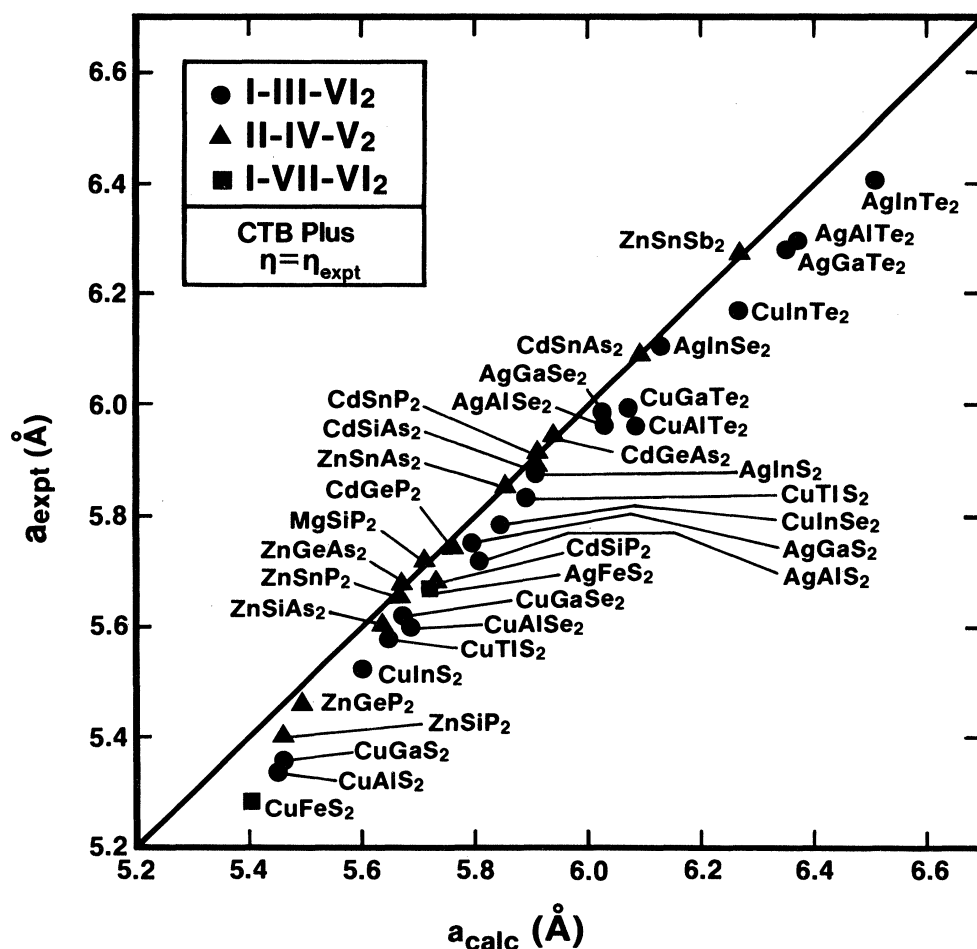
FIG. 19. Correlation between the observed and calculated lattice constants of ternary ABC_2 compounds using the "CTB plus $\eta = \eta_{expt}$ rule." The calculation is based on the Pauling tetrahedral radii of Table IV plus his radii of 1.40 and 1.23 Å for Mg and Fe, respectively.

δ. This highlights the significance of the chemical content of the distribution in anion displacement parameters (Table II) relative to the less sensitive distribution of lattice parameters a. It also explains,[58] in alloys of binary semiconductors (e.g., GaP-InP) which take up a local chalcopyrite arrangement, why the lattice constant closely obeys Vegard's rule ($a \simeq a_{ZB}$), whereas the two basic bond lengths remain unequal[60] ($u - \frac{1}{4} \neq 0$).

B. CTB plus $\eta = \eta_{tet}$ rule

An alternative approach to the problem is to add to Eqs. (4) a third condition that fixes η, namely the tetrahedral bond constraint around atom B given by Eq. (3). The solution to Eqs. (4) and (3) is then

$$a^2 = \frac{12\alpha^2}{2\beta + \alpha - [(2\beta + \alpha)^2 - 18\alpha^2]^{1/2}},$$

$$\eta^2 = \frac{8(\beta - \alpha)}{3a^2},$$

$$u = \frac{1}{2} - \frac{1}{4}[2\eta^2 - 1].$$

(10)

The power-series expansion in $\delta \equiv \alpha/\beta$ yields

$$a = \sqrt{8\beta/3}[1 + \delta/4 - \frac{3}{64}\delta^3 + O(\delta^4)],$$

$$\eta = 1 - \frac{3}{4}\delta + \frac{\delta^2}{16} - \frac{\delta^3}{16} + O(\delta^4),$$

(11)

$$u = \frac{1}{4} + \frac{3}{8}\delta + \frac{7}{64}\delta^2 + \frac{7}{32}\delta^3 + O(\delta^4).$$

This approach hence gives a, u, and η without recourse to any ternary compound experimental data. The predictions for the lattice constant a are compared with the experimental values in Fig. 21, and are seen to be of similar quality to those given by the CTB plus $\eta = \eta_{expt}$ rule (Fig. 19), since the bond lengths depend much more strongly on u than on η (i.e., the values of u and a that satisfy the bond-length—matching conditions are largely unaffected by the procedure used to fix η). The predictions for the anion displacements u given by the CTB plus $\eta = \eta_{tet}$ rule are so similar to those given by the CTB plus $\eta = \eta_{expt}$ rule (Fig. 20) that they are indistinguishable on the plot. The predicted η values are depicted in Fig. 22 showing only a mediocre correlation with the experimental values (in par-
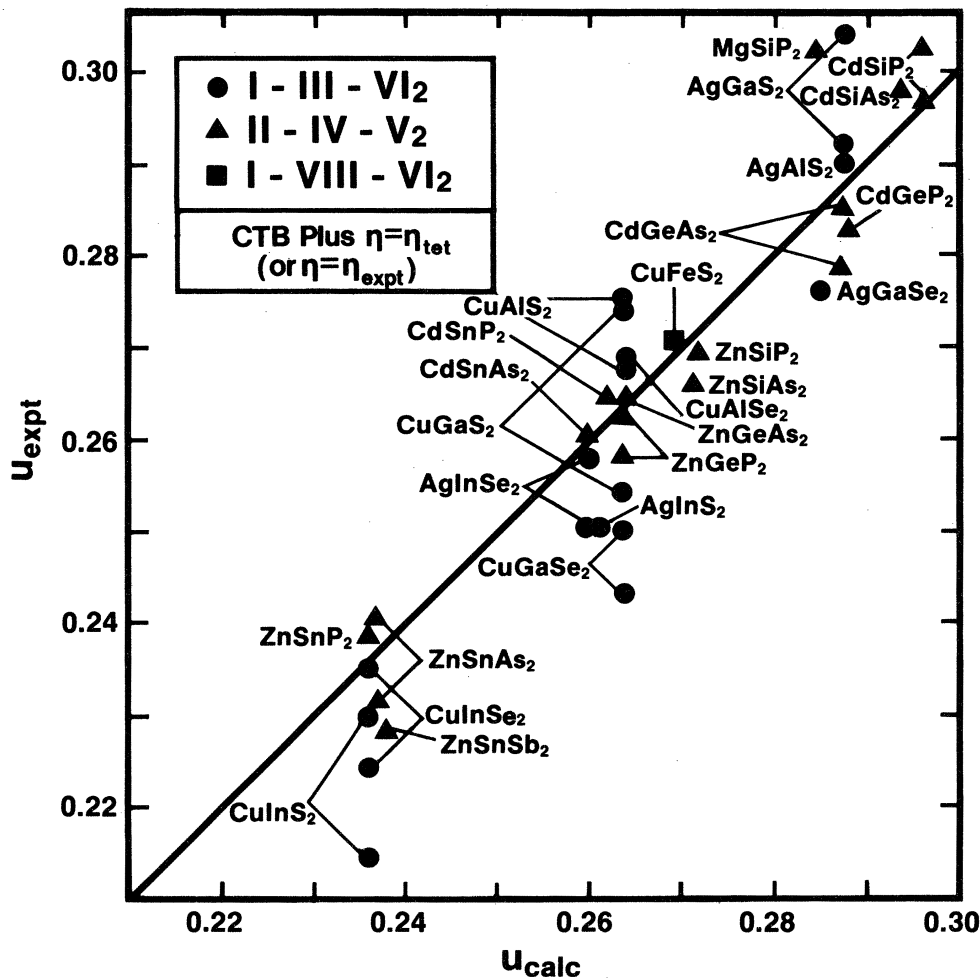
FIG. 20. Correlation between the observed and calculated anion displacement parameters of ternary ABC_2 compounds using the "CTB plus $\eta = \eta_{expt}$ rule." Very similar predictions for u are produced by the "CTB plus $\eta = \eta_{tet}$ rule." Multiple experimental values reflect the large disagreement between different authors' measurements. Values of u obtained by Hahn et al. (Ref. 27) are excluded as in Fig. 17.

TABLE IV. Comparison of the Shannon-Prewitt (SP) (Ref. 71) radii for the fourfold-coordinated cations and anions with Pauling's tetrahedral radii (Ref. 70).

Atom	SP radius (Å)	Pauling radius (Å)	Atom	Pauling radius (Å)
Cu^{1+}	0.635	1.35	Zn^{2+}	1.31
Ag^{1+}	0.92	1.52	Cd^{2+}	1.48
Al^{3+}	0.56	1.26	Si^{4+}	1.17
Ga^{3+}	0.58	1.26	Ge^{4+}	1.22
In^{3+}	0.765	1.44	Sn^{4+}	1.40
S^{2-}	1.70	1.04	P^{3-}	1.10
Se^{2-}	1.84	1.14	As^{3-}	1.18
Te^{2-}	2.07	1.32	Sb^{3-}	1.36

ticular for the compounds where $B=$ In, Tl, or Sn, where their tendency towards metallicity enables them to deviate substantially from directional tetrahedral bonding around the B site). Clearly, the CTB idea is not well suited for determining η, which is probably decided by longer-range electrostatic forces (rather than by local bond-strain effects); various effective electronegativity scales[62-65] might

indeed be more suited for systematizing η (see Ref. 64 in particular). Since, however, η variations are essentially inconsequential for understanding the band gaps of the materials, we will not dwell on this quantity further.

Our results suggest that the anion displacement parameters u and the lattice parameters a are fundamentally determined by the internal bond-length mismatch in these
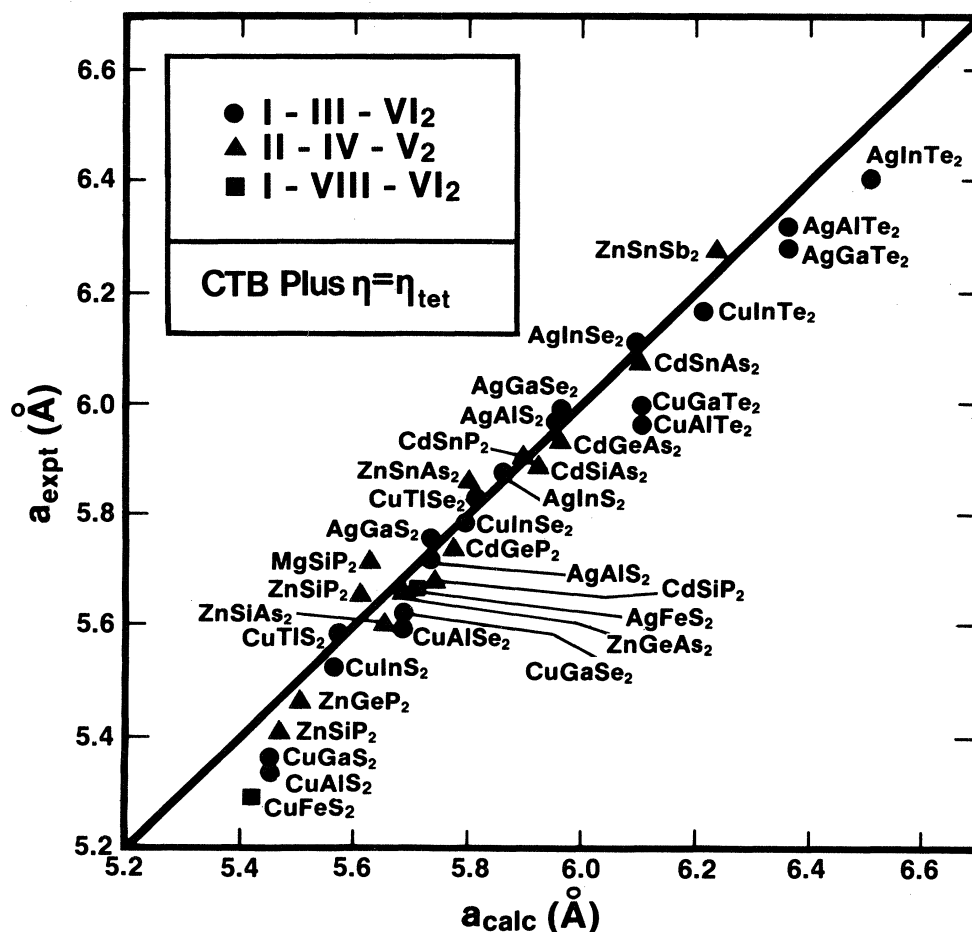
FIG. 21. Correlation between the observed and calculated lattice parameters of ternary ABC_2 chalcopyrites using the "CTB plus $\eta = \eta_{tet}$ rule," where no experimental data are needed as input.

compounds. One could certainly improve quantitatively on these correlations by replacing Pauling's tetrahedral radii by other radii determined from a larger data base of compounds, e.g., the Shannon-Prewitt (SP) radii.[71] Table IV compares the two set of radii for the elements for which both are available. The SP radii are larger for the anions but smaller (in a similar amount) for the cations, relative to Pauling's radii. However, the structure of the CTB equations indicate that this difference is trivial since a transformation $r_A \rightarrow r_A + \gamma$ and $r_C \rightarrow r_C - \gamma$ leaves the equations invariant. Table V shows that pairwise sums of the SP radii are, in most cases, closer to the experimental bond length than sums of Pauling radii. Table VI compares the predicted parameters a, u, and η from the CTB plus $\eta = \eta_{tet}$ rule using both the SP and Pauling's radii. Clearly, the SP radii do somewhat better than Pauling's radii. We have repeated these calculations with the Bragg-Slater[72] and Van Vechten—Phillips[73] radii, with worse results than with the Pauling radii.

VIII. SOME PREDICTIONS

The rules that we have provided can be used to determine fairly precisely the values of a and u and the band gap for compounds for which these have not been measured or for systems where the experimental scatter is too large. We show some of these predictions in Table VII. More importantly to our present work, these rules suggest that the anion displacements can be controlled empirically by alloying certain elements into given compounds, there-

by controlling the *optical gaps*, e.g., inclusion of Ga in $CuInSe_2$ is likely to increase the effective u, thereby opening the optical gap of the material. Such control of the optical gap is needed in many applications for optoelectric devices (e.g., for $CuInSe_2$ solar-cell applications, it is desirable to increase somewhat the ~ 1-eV gap of the material, to extract more energy per solar photon, and hence obtain a larger voltage across the solar cell[74]).

Table VII gives a list of some possible chalcopyrite-structure ternary semiconductors. Most of these have apparently never been synthesized; a few have been reported to exist [e.g., $AgTlSe_2$ (Ref. 8)], but without any crystallographic data being given. We have predicted the structural parameters (a, u, and η) for these 22 compounds using the CTB model with Pauling's tetrahedral covalent radii plus the condition $\eta = \eta_{tet}(u)$; our predictions should be considered more reliable for a and u than for η (Ref. 64). We also give rough estimates of the lowest band gaps E_g for the not-yet-synthesized compounds, based upon our theory of the band-gap anomaly. We expect that the lowest gaps will be direct ($\Gamma_{4v} \rightarrow \Gamma_{1c}$) for the I-III-VI$_2$ compounds and the larger-molecule-weight II-IV-V$_2$ compounds, while some of the lighter II-IV-V$_2$'s will have pseudodirect gaps; those most likely to be pseudodirect are so indicated in the table.

We have excluded from our list all those compounds that seem likely to have negative band gaps, since tetrahedral coordination becomes unstable as one passes from the semiconductor to the semimetal regime. Howev-
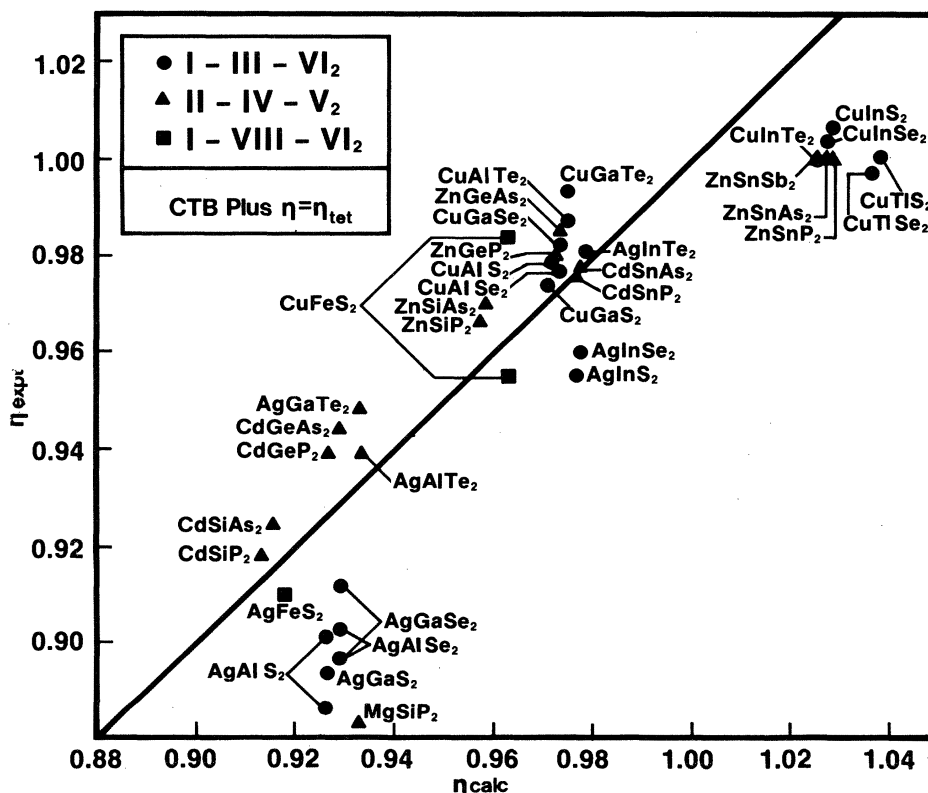
FIG. 22. Correlation between the observed and calculated tetragonal distortion parameters using the "CTB plus $\eta = \eta_{tet}$ rule" (where no data from the ternary compounds is used as input). Multiple experimental values are included only for the few cases where disagreements are substantial. The overall correlation is rather mediocre (see discussion in text).

TABLE V. Comparison of the experimental bond lengths (calculated from data of Table II) in ternary semiconductors to the sum of the Shannon-Prewitt (SP) (Ref. 71) radii and Pauling's (P) (Ref. 70) radii. Results given in Å; an asterisk denotes the approach that produces the better agreement with experiments.

Bond	Expt.	Compound	Calculated (SP)	Calculated (P)
Cu—S	2.374	$CuAlS_2$	2.335	2.39*
	2.312—2.380	$CuGaS_2$		
	2.288—2.334	$CuInS_2$		
Cu—Se	2.471	$CuAlSe_2$	2.475*	2.49
	2.387—2.417	$CuGaSe_2$	*	
	2.424—2.459	$CuInSe_2$	*	
Al—S	2.219	$CuAlS_2$	2.26*	2.30
	2.257	$AgAlS_2$	*	
Al—Se	2.347	$CuAlSe_2$	2.40	2.40
Ga—S	2.224—2.288	$CuGaS_2$	2.28*	2.30
	2.235—2.276	$AgGaS_2$	*	
Ga—Se	2.400—2.417	$CuGaS_2$	2.42	2.40
	2.416	$AgGaSe_2$	*	
In—S	2.465—2.517	$CuInS_2$	2.465	2.48
	2.505	$AgInS_2$		*
In—Se	2.559—2.598	$CuInSe_2$	2.605	2.58
	2.609—2.638	$AgInSe_2$	*	
Ag—S	2.530	$AgAlS_2$	2.62	2.56*
	2.556—2.605	$AgGaS_2$		
	2.505	$AgInS_2$		*
Ag—Se	2.601	$AgGaSe_2$	2.76	2.66*
	2.578—2.609	$AgInSe_2$		*

er, the chalcopyrite structure should be a reasonable prediction for the remaining compounds in view of the existence of zinc-blende-structure compounds containing these same elements in the same or in different combinations. An example is $MgGeP_2$, which has been synthesized[61] in a cation-disordered zinc-blende phase with

$a = 5.652$ Å, in good agreement with our prediction; it should be possible to obtain this compound as a chalcopyrite by extremely slow cooling from near its melting point. As another example, one can argue for the existence of Hg-containing chalcopyrites from the existence of a zinc-blende phase of HgSe. On the other hand, ternary nitrides

TABLE VI. Comparison of predicted a, u, and η parameters from the "CTB plus $\eta = \eta_{tet}$ rule," using the Shannon-Prewitt (SP) radii and the Pauling (P) radii. An asterisk denotes the one that produces better agreement with experiment.

Compound		u			a (Å)			η	
	Expt.	SP	P	Expt.	SP	P	Expt.	SP	P
$CuAlS_2$	0.2750	0.2621	0.2641*	5.3340	5.3466*	5.4639	0.9790	0.9762*	0.9721
$CuAlSe_2$	0.2690	0.2614	0.2636*	5.6020	5.6700*	5.6950	0.9770	0.9775*	0.9732
$CuGaS_2$	0.2539—	0.2588	0.2641	5.3474—	5.3593*	5.4639	0.9740—	0.9825	0.9721
	0.2750			5.356			0.9794		
$CuGaSe_2$	0.2431—	0.2583*	0.2636	5.5963—	5.6827*	5.6950	0.9800—	0.9835*	0.9732
	0.2500			5.6140			0.9831	*	
$CuInS_2$	0.2140—	0.2291*	0.2359	5.5228—	5.4595	5.5677*	1.0025—	1.0427	1.0287*
	0.2295			5.5230			1.0079		
$CuInSe_2$	0.2240—	0.2303	0.2364	5.7730—	5.7833*	5.7988	1.0005—	1.0402	1.0275*
	0.2350			5.7840			1.0048		

TABLE VII. Predicted structural parameters and estimated band gaps for 22 possible chalcopyrite-structure semiconductors. The symbol PD in the band-gap column indicates compounds most likely to have pseudodirect lowest gaps.

Compound	a (Å)	u	η	E_g (eV)
ZnSiSb$_2$	6.077	0.270	0.961	0.9
ZnGeSb$_2$	6.111	0.263	0.975	0.5
CdSiSb$_2$	6.344	0.291	0.921	0.8
CdGeSb$_2$	6.383	0.285	0.933	0.2
MgGeP$_2$	5.656	0.277	0.947	2.1 (PD)
MgSnP$_2$	5.774	0.250	1.000	1.8
MgSiAs$_2$	5.804	0.284	0.935	2.0 (PD)
MgGeAs$_2$	5.841	0.276	0.949	1.6
MgSnAs$_2$	5.958	0.250	1.000	1.2
MgSiSb$_2$	6.221	0.281	0.939	1.4
MgSeSb$_2$	6.258	0.275	0.952	0.9
MgSnSb$_2$	6.374	0.250	1.000	0.6
HgSiP$_2$	5.740	0.296	0.913	1.6
HgGeP$_2$	5.780	0.288	0.927	1.2
HgSnP$_2$	5.909	0.262	0.977	0.8
HgSiAs$_2$	5.926	0.294	0.916	0.7
HgGeAs$_2$	5.966	0.287	0.929	0.2
CuTlTe$_2$	6.299	0.233	1.034	0.9
AgTlS$_2$	5.882	0.257	0.986	1.1
AgTlSe$_2$	6.113	0.257	0.986	0.7, 0.72[a]
AgTlTe$_2$	6.529	0.257	0.987	0.6
BeCN$_2$	3.847	0.313	0.883	8.2 (PD)

[a]Experimental value, Ref. 8, p. 336.

like ZnGeN$_2$ are known[75] to have a structure related to wurtzite, which is not surprising since their binary analogs (e.g., GaN) have the wurtzite structure. But the tetrahedrally coordinated form of boron nitride (BN) appears also in the zinc-blende structure, which suggests that BeCN$_2$ may exist in a chalcopyrite structure. This ternary analog of diamond might have properties approximating those of diamond itself.

The connection we have demonstrated between anion sublattice distortion and the band-gap anomaly may help to answer some questions about alloys of chalcopyrite compounds. For example, it is has been show that when one has solid solutions of two different anions in the chalcopyrite lattice [e.g., CuInS$_2$Se$_{2(1-x)}$ (Refs. 76 and 77), CuGaS$_{2x}$Se$_{2(1-x)}$ (Ref. 78), and ZnSiP$_{2x}$As$_{2(1-x)}$ (Ref. 79)], then the band gap is always almost exactly linear in the composition parameter x, i.e., there is little or no optical bowing in these alloys. On the other hand, when there is alloying on the B cation [as in CuGa$_x$In$_{1-x}$Se$_x$ (Ref. 80)] or on the A cation [as in Ag$_x$Cu$_{1-x}$InSe$_2$ (Ref. 77)], then substantial optical bowing is usually (though not always[81]) found. We suggest that the difference between these two cases is partly due to the behavior of the anion displacement parameter with alloying, where we assume that the structure of the alloy is approximately described by a concentration-dependent $u(x)$. Specifically, inspec-

tion of Eqs. (9) and (11) shows that changes in the parameter u are dominated by changes in the term that is linear in the small ratio δ, and it is easily shown that δ depends much more strongly on the cation radii r_A and r_B than on the anion radius r_C. We take these radii to have concentration-dependent effective values in the alloy, and define

$$Q = 4R_{AC}R_{BC}/\beta^2 . \tag{12}$$

Then we have

$$\frac{\partial \delta}{\partial r_A} = R_{BC}Q , \quad \frac{\partial \delta}{\partial r_B} = R_{AC}Q ,$$

$$\frac{\partial \delta}{\partial r_C} = (R_{BC} - R_{AC})Q = (r_B - r_A)Q . \tag{13}$$

The difference $r_A - r_B$ is about 8–30 times smaller in absolute magnitude than either bond length; thus, the anion radius has relatively little influence on u. (This can also be seen by examining our predicted values of u for series such as ABS$_2$, ABSe$_2$, and ABTe$_2$.) Now we have seen that u controls the structural part ΔE_g^S of the band-gap anomaly, and this suggests that alloying the anions will not substantially affect ΔE_g^S. On the other hand, since the cation radii strongly affect u and hence ΔE_g^S, alloying with either the A or B atom should have a strong structural effect on the band gap, especially if the size mismatch between alloyed (same-column) elements is large. If either the concentration dependence $u(x)$ of the anion positions or the variation $E_g(u)$ of the gap is nonlinear, there will be a structurally induced bowing ($E_g[u(x)]$ $\neq x E_g[u(1)] + (1-x)E_g[u(0)]$ when $0 < x < 1$) that is not present when only the anions are alloyed.

IX. SUMMARY

We have proposed a theory for the band-gap anomaly, structural deformations, and the relationship between them for ternary ABC_2 chalcopyrites. We find that the band-gap anomaly can be analyzed in terms of a chemical factor ΔE_g^{chem} and a structural factor ΔE_g^S, where

$$\Delta E_g = \Delta E_g^{chem} + \Delta E_g^S .$$

The chemical contribution to the band-gap anomaly consists of a d-p hybridization part ΔE_g^d and a cation electronegativity part ΔE_g^{CE},

$$\Delta E_g^{chem} = \Delta E_g^d + \Delta E_g^{CE} .$$

ΔE_g^d reflects the raising of the VBM due to the level repulsion between the cation d orbitals and the anion p orbitals, both forming Γ_{15}-like representatives. This effect is small in II-VI and III-V compounds where the cation d orbitals (Zn, Cd, Ga, and In) are considerably deeper than the anion p orbitals, but is significant in Cu-based chalcopyrites and in Cu-based binary compounds (e.g., CuCl), and also, to a lesser extent, in the corresponding Ag compounds. The p-d hybridization effect is also responsible for the occurrence of anomalously deep Cu acceptor states in II-VI compounds, relative to the shallow acceptor states in III-V and column-IV semiconductors. The CE factor ΔE_g^{CE} reflects the ability of charge to

separate on the two cation sublattices in ternary compounds. It is a significant factor for III-V alloys (e.g., GaP-InP) but small in ternary chalcopyrites relative to the other factors.

The structural contribution ΔE_g^S to the band-gap anomaly is controlled by bond alternation (i.e., $R_{AC} \neq R_{BC}$, or $u - \frac{1}{4} \neq 0$) and has only a small contribution from tetragonal distortions ($\eta = c/2a \neq 1$). We show that bond alternation can have either a positive or a negative contribution to ΔE_g and that a large fraction of the optical bowing phenomena in conventional binary alloys (e.g., InP-GaP) is a consequence of bond alternation (i.e., the breakdown of the virtual-crystal approximation). We have analyzed in detail the rearrangements in charge distribution due to bond alternation and identified the charge-polarization effects associated with it.

We find that ΔE_g^S has a term linear in the anion distortion $u - \frac{1}{4}$ with a linear coefficient that depends on the electronegativity difference between the cations (i.e., one that vanishes for zinc-blende compounds) and a term quadratic in $u - \frac{1}{4}$ with a coefficient that depends on the average CE (i.e., similar for ternary and the analogous

binary compounds). We suggest that most of ΔE_g^S for chalcopyrites arises from the linear term, whereas most of the structurally induced optical bowing in alloys of binary semiconductors arises from the quadratic term.

Finally, we show that the observed distribution of lattice parameters a and anion displacement parameters u in ternary ABC_2 semiconductors can be systematized through a semiclassical model of conservation of tetrahedral bonds. This model also provides predictions for a, u, and E_g for compounds that have not been synthesized yet. The present model of the band-gap anomaly and the structure anomalies in ternary semiconductors are being used in our laboratory for guiding the design of new ternary compounds and alloys with desired band gaps and lattice constants for photovoltaic applications.

ACKNOWLEDGMENTS

[1]E. Parthé, Crystal Chemistry of Tetrahedral Structures (Gordon and Breach, New York, 1964).

[2]N. A. Goryunova, The Chemistry of Diamond-Like Semiconductors (Chapman and Hall, New York, 1965).

[3]J. L. Shay and J. H. Wernick, Ternary Chalcopyrite Semiconductors: Growth, Electronic Properties and Applications (Pergamon, Oxford, 1974).

[4]U. Kaufmann and J. Schneider, in Festkörperprobleme XIV, edited by J. Treusch (Vieweg, Braunschweig, 1974), p. 229.

[5]S. Wagner, in Electroluminescence, edited by J. O. Pankove (Springer, Berlin, 1977), p. 171.

[6]A. MacKinnon, in Festkörperprobleme XXI, edited by J. Treusch (Vieweg, Dortmund, 1981), p. 149.

[7]A. Miller, A. MacKinnon, and D. Weaire, in Solid State Physics, edited by H. Ehrenreich, F. Seitz, and D. Turnbull, (Academic, New York, 1981), Vol. 36.

[8]B. R. Pamplin, T. Kiyosawa, and K. Masumoto, Prog. Cryst. Growth Charact. 1, 331 (1979).

[9]S. Wagner, J. L. Shay, P. Migliorato, and H. M. Kasper, Appl. Phys. Lett. 25, 434 (1974).

[10]L. L. Kazmerski and Y. J. Juang, J. Vac. Sci. Technol. 14, (1977).

[11]R. A. Mickelsen and W. S. Chen, in Fifteenth IEEE Photovoltaic Specialists Conference, 1981, IEEE Publication No. 81CH1644-4, p. 800.

[12]W. Hörig, H. Neumann, H. Sobotta, B. Schumann, and G. Kühn, Thin Solid Films 48, 67 (1978).

[13]Data for GaAs, M. D. Sturge, Phys. Rev. 127, 768 (1962); for CdS, D. Dutton, Phys. Rev. 112, 785 (1958); for Zn_3P_2, E. A. Fagen, J. Appl. Phys. 50, 6505 (1979); for CdTe, K. Mitchell, A. L. Fahrenbruch, and R. H. Bube, J. Appl. Phys. 48, 829 (1977); for Cu_2S, B. J. Mulder, Phys. Status Solidi A 13, 79 (1972); for a-SiH, G. D. Cody, C. R. Wronski, B. Abeles, R. B. Stephens, and B. Brooks, Solar Cells 2, 227 (1980); for crystalline (c)- Si, H. A. Weakleim and D. Redfield, J. Appl. Phys. 50, 1491 (1979). We are grateful to J. Meakin for a compilation of part of these data.

[14]R. E. Bird and R. L. Hulstrom, Terrestrial Solar Spectral Data Sets, SERI/TR-642-1149, June, 1982 (unpublished). Here, "Air Mass 1.5" indicates a typical spectrum incident on a flat-plate photovoltaic array.

[15]J. L. Shay, B. Tell, H. M. Kasper, and L. M. Schiavone, Phys. Rev. B 5, 5003 (1972).

[16]B. Tell, J. L. Shay, and H. M. Kasper, Phys. Rev. B 4, 2463 (1971).

[17]M. Bettini, Solid State Commun. 13, 599 (1973).

[18]J. L. Shay, B. Tell, H. M. Kasper, and L. M. Schiavone, Phys. Rev. B 7, 4485 (1973).

[19]W. N. Honeyman and K. H. Wilkinson, J. Phys. D 4, 1182 (1971).

[20]H. Neumann, W. Hörig, E. Reccius, H. Sabotta, B. Schumann, and G. Kühn, Thin Solid Films 61, 13 (1979).

[21]M. J. Thwaites, R. D. Tomlinson, and M. J. Hampshire, in Ternary Compounds 1977, edited by G. D. Holah (Institute of Physics, London, 1977), p. 237.

[22]B. Tell, J. L. Shay, and H. M. Kasper, Phys. Rev. B 6, 3008 (1972).

[23]W. H. Strehlow and E. L. Cook [J. Phys. Chem. Ref. Data 2, 163 (1973)] gives a compilation of energy-band gaps of binary materials. We use the data corresponding to the same temperature used for the ternary materials.

[24]J. E. Jaffe and A. Zunger, Phys. Rev. B 27, 5176 (1983).

[25]Some of the gaps given in Table I of Ref. 24 have been refined here using more accurate experimental data (i.e., for $CuAlSe_2$, $CuGaTe_2$, and $CuInTe_2$).

[26]J. E. Jaffe and A. Zunger, Phys. Rev. B 28, 5822 (1983).

[27]H. Hahn, G. Frank, W. Klingler, A. Meyer, and G. Storger, Z. Anorg. Chem. 271, 153 (1953).

[28]H. W. Spiess, V. Haeberln, G. Brandt, A. Rauber, and J. Schneider, Phys. Status Solidi B 62, 183 (1974).

[29]G. Brandt, A. Rauber, and J. Schneider, Solid State Commun. 12, 481 (1973).

[30]S. C. Abrahams and J. L. Bernstein, J. Chem. Phys. 59, 5415 (1973).

[31]J. Schneider, A. Rauber, and G. Brandt, J. Phys. Chem. Solids 34, 443 (1973).

[32]S. C. Abrahams and J. L. Bernstein, J. Chem. Phys. 61, 1140 (1974).

[33]J. Parkes, R. D. Tomlinson, and M. J. Hampshire, J. Appl. Cryst. 6, 414 (1973).

[34]S. C. Abrahams and J. C. Bernstein, J. Chem. Phys. 59, 1625 (1973).

[35]P. Benoit, P. Charpin, R. Lesueur, and C. Djaga-Mariadassou, in Proceedings of the Fourth International Conference on Ternary and Multinary Semiconductors, Tokyo, 1980 [Jpn. J. Appl. Phys. Suppl. 19-3, 85 (1980)].

[36]Handbook of Chemistry and Physics, 63rd ed., edited by R. C. Weast and M. J. Astle, (Chemical Rubber Co., Boca Raton, Fla., 1982), p. B-121.

[37]S. C. Abrahams and J. L. Bernstein, J. Chem. Phys. 52, 5607 (1970).

[38]A. A. Vaipolin, Fiz. Tverd. Tela 15, 1430 (1973) [Sov. Phys.—Solid State 15, 965 (1973)].

[39]M. D. Lind and R. W. Grant, J. Chem. Phys. 58, 357 (1973).

[40]A. A. Vaipolin, N. A. Goryusova, L. I. Kleshchinskii, G. V. Loshakova, and E. D. Osmanov, Phys. Status Solidi 29, 435 (1968).

[41]H. Pfister, Acta Crystallogr. 16, 153 (1963).

[42]D. B. Gasson, P. J. Holmes, I. C. Jennings, B. R. Marathe, and J. E. Parrott, J. Phys. Chem. Solids 23, 1291 (1962).

[43]A. A. Vaipolin, L. V. Kradinova, and V. D. Prochukhan, Kristallografiya 15, 820 (1970) [Sov. Phys.—Crystallogr. 15, 703 (1971)].

[44]S. C. Abrahams and J. L. Bernstein, J. Chem. Phys. 55, 796 (1971).

[45]B. B. Sharma, A. A. Vaipolin, and Yu. A. Valo, Zh. Strukt. Khim. 11, 781 (1970).

[46]R. Grigorovici, R. Manaila, and A. A. Vaipolin, Acta Crystallogr. Sect. B 24, 535 (1968).

[47]H. Pfister, Acta Crystallogr. 11, 221 (1958).

[48]A. A. Vaipolin, E. O. Osmanov, and Yu. V. Rud, Fiz. Tverd. Tela 7, 7765 (1965) [Sov. Phys.—Solid State 7, 1833 (1966)].

[49]P. Bendt and A. Zunger, Phys. Rev. B 26, 3114 (1982).

[50]D. M. Ceperley and B. J. Alder, Phys. Rev. Lett. 45, 566 (1980).

[51]D. M. Ceperley, Phys. Rev. B 18, 3126 (1978).

[52]J. P. Perdew and A. Zunger, Phys. Rev. B 23, 5048 (1981).

[53]D. M. Wood and A. Zunger (unpublished).

[54]A. Zunger, J. Perdew, and G. Oliver, Solid State Commun. 34, 933 (1980).

[55]J. L. Shay and H. M. Kasper, Phys. Rev. Lett. 29 1162 (1972); in Ternary Chalcopyrite Semiconductors: Growth, Electronic Properties and Applications, Ref. 3, p. 118.

[56]Y. S. Park and B. K. Shin, in Electroluminescence, edited by J. I. Pankove (Springer, Berlin, 1977), p. 133.

[57]Landolt-Börnstein Zahlenwerte und Funktionen aus Naturwissenschaften and Technik, New Series, edited by K. H. Hellwege (Springer, Berlin, 1982), Vol. 17, p. 64.

[58]A. Zunger and J. E. Jaffe, Phys. Rev. Lett. 51, 662 (1983).

[59]See reviews in (a) A. Onton, Festkörperprobleme (Vieweg, Braunschweig, 1973), Vol. XIII, p. 59; (b) D. Long, in Semiconductors and Semimetals, edited by R. K. Willardson and A. C Beer (Academic, New York, 1966), p. 143; (c) T. P. Pearsall, in GaInAsP Alloy Semiconductors, edited by T. P. Pearsall (Wiley, New York, 1982), p. 295.

[60]J. C. Mikkelsen and J. B. Boyce, Phys. Rev. Lett. 49, 1412 (1983).

[61]O. G. Folberth and H. Pfister, Acta Crystallogr. 13, 199 (1960).

[62]J. C. Phillips, J. Phys. Chem. Solids 35, 1205 (1974).

[63]J. R. Chelikowsky and J. C. Phillips, Phys. Rev. B 17, 2453 (1978).

[64]A. Shaukat and R. D. Singh, J. Phys. Chem. Solids 39, 1269 (1978). These authors displayed η as a function of the electronegativity difference $X_A - X_B$ defined through empirical orbital radii [J. St. John and A. N. Bloch, Phys. Rev. Lett. 33, 1095 (1974)]. We note here that using instead the nonempirical density-functional orbital radii [A. Zunger, Phys. Rev. Lett. 44, 582 (1980); ibid. Phys. Rev. B 22, 5839 (1980)], and the same definitions of electronegativities X_A and X_B produces a far better correlation with η, both for I-III-VI$_2$ and for II-IV-V$_2$ compounds. The correlation is superior also to that of Refs. 62 and 63 and is predictive for alloys of ternary materials.

[65]J. Noolandi, Phys. Rev. B 10, 2490 (1974).

[66]E. R. DeGil, Phys. Status Solidi (a) 70, 519 (1982).

[67]G. C. Bhar and L. K. Samanta, Phys. Rev. B 26, 2275 (1982).

[68]W. L. Bragg, Philos. Mag. 40, 169 (1920).

[69]D. S. Chemla, A. Deschanvres, and B. Mercey, J. Phys. (Paris) Colloq. 36, C3-17 (1975).

[70]L. Pauling, The Nature of the Chemical Bond (Cornell University Press, Ithaca, New York, 1967), p. 246.

[71]See the review by R. D. Shannon, in Structure and Bonding in Crystals, edited by M. O'Keefe and A. Navrotsky (Academic, New York, 1981), Vol. II, p. 53.

[72]J. C. Slater, Symmetry and Energy Bands in Crystals (Dover, New York, 1965), p. 55.

[73]J. A. Van Vechten and J. C. Phillips, Phys. Rev. B 2, 2160 (1970).

[74]H. J. Hovel, in Semiconductors and Semimetals, Vol. 11: Solar Cells, edited by R. K. Willardson and A. C. Beer (Academic, New York, 1975), pp. 71ff.

[75]M. Maunaye and J. Lang, Mater. Res. Bull. 5, 793 (1970).

[76]I. V. Bodnar, B. V. Kozun, and A. J. Lakomskii, Phys. Status Solidi (b) 105, K143 (1981).

[77]C. H. Chapman, J. Schewchun, J. J. Loferski, B. K. Garside, and R. Beaudieu, Appl. Phys. Lett. 34, 735 (1979).

[78]G. Goodchild, J. C. Woolley, and J. Gonzales, Proceedings of the Fourth International Conference on Ternary and Multinary Semiconductors, Tokyo, 1980, Ref. 34, p. 123.

[79]J. Gallay, A. Deschenvres, S. Gaillard, and C. Alibert, J. Phys. (Paris) Colloq. 36, C3-123 (1975).

[80]I. V. Bodnar, A. P. Bologa, and B. V. Korzun, Phys. Status Solidi B 109, K31 (1982).

[81]W. Hörig, W. Möller, H. Neumann, E. Reccius, and G. Kühn, Phys. Status Solidi B 92, K1 (1979).